Title
Exact Solutions of Frustrated Ordinary and Chiral Eight-Site Hubbard Models

Journal
Physical review B, 44(4)

Authors
Freericks, J.K.
Falicov, L.M.
Rokhsar, D.S.

Publication Date
1991-02-01

LBL-30344
Preprint

Lawrence Berkeley Laboratory
UNIVERSITY OF CALIFORNIA

Materials & Chemical Sciences Division

Submitted to Physical Review B

Exact Solutions of Frustrated Ordinary and Chiral Eight-Site Hubbard Models

J.K. Freericks, L.M. Falicov, and D.S. Rokhsar

February 1991

Prepared for the U.S. Department of Energy under Contract Number DE-AC03-76SF00098.

DISCLAIMER

LBL-30344

EXACT SOLUTIONS OF FRUSTRATED ORDINARY AND CHIRAL EIGHT-SITE HUBBARD MODELS*

J. K. Freericks and L. M. Falicov

Department of Physics
University of California
Berkeley, CA 94720

and

Materials Sciences Division
Lawrence Berkeley Laboratory
Berkeley, CA 94720

and

D. S. Rokhsar

Department of Physics
University of California
Berkeley, CA 94720

February 1991

---

*This work was supported in part by the Director, Office of Energy Research, Office of Basic Energy Sciences, Materials Sciences Division of the U. S. Department of Energy under Contract No. DE-AC03-76SF00098.

Exact Solutions of Frustrated Ordinary and Chiral Eight-Site Hubbard Models

J. K. Freericks and L. M. Falicov

Department of Physics,
University of California,
Berkeley, CA 94720,

and

Materials Science Division,
Lawrence Berkeley Laboratory,
Berkeley, CA 94720,

and D. S. Rokhsar

Department of Physics,
University of California,
Berkeley, CA 94720.

ABSTRACT

This contribution addresses the question of whether or not the ground state of a frustrated spin-1/2 Heisenberg model can be smoothly related to the ground state of a simple tight-binding model at half-filling in an appropriately chosen magnetic field. This continuity is considered explicitly for an eight-site square-lattice Hubbard model with nearest- and next-nearest-neighbor hopping, which approaches a frustrated Heisenberg model with nearest- and next-nearest-neighbor antiferromagnetic exchange coupling in the limit of large Hubbard U. In addition, a counterexample to the folklore that the half-filled band of the ordinary Hubbard model is nonmagnetic has been found in the regime where the hopping parameters and Hubbard interaction are all the same order of magnitude.

1990 PACS number(s): 75.10.Lp, 74.65.+n, 71.28.+d

Exact Solutions of Frustrated Ordinary and Chiral Eight-Site Hubbard Models

J. K. Freericks and L. M. Falicov

Department of Physics,
University of California,
Berkeley, CA 94720,

and

Materials Science Division,
Lawrence Berkeley Laboratory,
Berkeley, CA 94720,

and D. S. Rokhsar

Department of Physics,
University of California,
Berkeley, CA 94720.

I. Introduction

Although the ground states of the Mott-insulating progenitors of high-temperature superconductors display long-range antiferromagnetic order, it has been suggested that hypothetical "spin-liquid" or "resonating-valence-bond" states which are translationally and spin-rotationally invariant may hold the key to the mechanism of oxide superconductivity[1–3]. These states possess short-range spin correlations which mimic the short-range spin correlations in a singlet superconductor, and may therefore serve as an appropriate starting point for understanding the nature of superconductivity in doped Mott insulators. The excitation spectrum of these spin liquids is supposed to contain quasiparticles with reversed spin-charge-relations — the neutral spin-1/2 "spinon" and the spinless charge-e "holon" — and the superconducting ground state is thought of as a condensate of holons.

Despite the theoretical interest in spin liquids, it has proven difficult to identify a particular frustrated spin-1/2 Heisenberg model with a spin-liquid ground state. The

search for these states is complicated by the difficulty of solving frustrated spin models on infinite lattices (or lattices which are large enough to render boundary effects unimportant), especially in view of the possibility of incommensurable spin-density-wave ground states. The understanding of spin liquids is therefore largely based on approximate methods which fall into three different categories: (a) mean-field theories; (b) variational and projection techniques; and (c) small-cluster (finite-system) exact calculations.

I(a) **Mean-Field Theories.** Conventional mean-field theory for antiferromagnets (AF), in which the spin at every site acquires a nonzero expectation value, is not appropriate for the study of spin liquids, since they are by hypothesis spin-rotationally invariant. Affleck and Marston[4] have proposed an alternative mean-field theory by recalling that antiferromagnetic exchange between two spins at sites i and j arises from the virtual hop of an electron from site i to site j and back again, *viz.*, $[-2J_{ij}(c_{i\sigma}^{\dagger}c_{j\sigma})(c_{j\tau}^{\dagger}c_{i\tau})]$. This expression leads naturally to the introduction of the (possibly complex) link variables $\chi_{ij} \equiv (J_{ij}/2) <c_{j\sigma}^{\dagger}c_{i\sigma}>$ and the corresponding mean-field Hamiltonian

$$H_{MF} = \sum_{(i,j)} \frac{|\chi_{ij}|^2}{J_{ij}} + \sum_{(i,j),\,\sigma} [\chi_{ij}\, c_{i\sigma}^{\dagger}\, c_{j\sigma} + \chi_{ij}^{*}\, c_{j\sigma}^{\dagger}\, c_{i\sigma}] \quad . \tag{1}$$

The mean-field state is obtained by minimizing H_{MF} with respect to the link variables χ_{ij}, a procedure which yields exact results for the $SU(N)$ Heisenberg model in the large-N limit. The ground state in the mean-field approximation is then the Slater determinant obtained by filling the single-particle states in the lower half of the spectrum of (1). Since the effective hopping amplitudes χ_{ij} are generally complex, the Hamiltonian (1) is equivalent to a system of noninteracting fermions moving in a "magnetic field" which couples only to *orbital* motion. The mean-field Hamiltonian (1) preserves an important symmetry of the Heisenberg model, namely the local $U(1)$

gauge symmetry associated with the conservation of particle number at each site[5]. Under a local gauge transformation, $c_{j\sigma}^{\dagger} \rightarrow \exp(i\Lambda_j)c_{j\sigma}^{\dagger}$, every state in the Hilbert space of the Heisenberg model is multiplied by the same overall phase factor $\exp(i\Sigma_j\Lambda_j)$ and therefore all observables are unaffected.

In general H_{MF} is minimized[6] by states with nonzero χ_{ij} only on isolated links of the lattice. To obtain stable translationally invariant spin-liquids in a mean-field approximation one may introduce biquadratic spin-spin interactions[4] which suppress fluctuations of the magnitudes $|\chi_{ij}|$. The resulting states have uniform (but fluctuating) charge density.

I(b) **Variational and Projection Techniques.** Slater determinants such as the mean-field states described above can be converted into suitable variational wavefunctions for the Heisenberg model by progressively eliminating those components of the Slater determinant which correspond to multiple occupancy of sites — the "Gutzwiller" technique. These projected wavefunctions yield excellent variational energies[7] (and therefore accurately describe short-range correlations) when the "flux" through every elementary plaquette $(ijkl)$ is π, *i.e.*, when the phase of the product $\chi_{ij}\chi_{jk}\chi_{kl}\chi_{li}$ of the link variables around the plaquette is π. On a square lattice with diagonal (frustrating) interactions, the optimal state (with uniform $|\chi_{ij}|$) is the "chiral" state[3,8], with flux $\pi/2$ through each elementary triangle, which breaks both time-reversal and parity symmetries.

The philosophy behind the Gutzwiller approach is a familiar one. To study a strongly interacting many-body system, one first identifies a simpler weak-coupling limit which embodies the same symmetries, and then imagines a smooth deformation of this soluble model into the intractable Hamiltonian under consideration. If no phase transition or level crossing intervenes, then the two opposite limits will be qualitatively similar. In some cases, the smooth continuation from weak to strong coupling can be

convincingly demonstrated. An instructive example of such a continuum of models is the half-filled, square-lattice Hubbard model with nearest-neighbor-only hopping[9]. In the small Hubbard U limit, this system is a commensurable spin-density-wave insulator, with an exponentially small charge gap. In the opposite (large Hubbard U) limit, charged excitations can be formally eliminated, resulting in a nearest-neighbor Heisenberg AF with a Néel-ordered ground state. In both cases, the ground-state density correlations decay exponentially, and the low-energy, long-wavelength excitations are gapless antiferromagnons. Despite the apparent conceptual difference between a commensurable spin-density-wave insulator (whose charge gap is caused by a doubling of the unit cell), and a Néel-ordered Mott insulator (whose gap is generally viewed as a many-body effect), there appears to be no phase-boundary separating them. The use of Gutzwiller-projected wavefunctions tacitly assumes a smooth interpolation of ground states from weak to strong coupling. If these two limits can be continuously related, the Gutzwiller approach provides a crude but powerful approximation for discussing strongly interacting problems using weak-coupling methods.

If the proposed spin-liquid states do indeed exist as ground states of an appropriately frustrated spin model, one may ask whether or not a smooth continuation to a more easily studied weak-coupling model exists. In particular, the mean-field theory of equation (1) suggests[10] a clear possible starting point: a Hubbard model in the presence of an arbitrary magnetic field which couples only to orbital motion, *i.e.*,

$$H = -\sum_{i,j,\sigma} t_{ij}\, c_{i\sigma}^{\dagger}\, c_{j\sigma} + U \sum_{i} n_{i\uparrow} n_{i\downarrow} \quad ,$$

$$t_{ij} \equiv T_{ij}\, e^{i\phi_{ij}} \quad ; \quad t_{ij} = t_{ji}^{*} \quad , \tag{2}$$

where $n_{i\sigma} = c_{i\sigma}^{\dagger}\, c_{i\sigma}$ is the particle number at site i, the T_{ij} are real and positive, and hopping is not limited to nearest-neighbors. At half-filling and in the large-U limit, for *any* choice of link phases $\{\phi_{ij}\}$, this Hubbard model approaches a frustrated spin-1/2 Heisenberg model in which the ratios J_{ij}/J_{kl} are simply $(T_{ij}/T_{kl})^2$. Each set of

link phases therefore specifies a family of Hamiltonians which interpolates between different soluble models ($U = 0$) and one intractable spin model ($U = \infty$). If for a sufficiently clever choice of phases it is possible to interpolate smoothly between the two limits, then one can infer properties of the frustrated Heisenberg model from a careful study of tight-binding independent-particle models.

For a generic choice of hopping phases ϕ_{ij}, the model described by the Hamiltonian (2) explicitly breaks time-reversal and parity symmetries. For large U this is reflected in the fact that the corresponding Heisenberg model includes three-spin interactions[10]

$$\sum_{ijk} \frac{T_{ij}\, T_{jk}\, T_{ki}}{U^2} \sin[\Phi_{ijk}]\ \mathbf{S}_i \cdot \mathbf{S}_j \times \mathbf{S}_k \quad , \tag{3}$$

where $\Phi_{ijk} \equiv \phi_{ij} + \phi_{jk} + \phi_{ki}$ is the flux through triangle ijk. These terms vanish in the Mott limit, since they are smaller by a factor of (T/U) than the usual quadratic spin-spin Heisenberg coupling $[(4T_{ij}^2/U)\ \mathbf{S}_i \cdot \mathbf{S}_j]$. They may, however, act as infinitesimal symmetry-breaking fields (in the large-U limit) if the ground state of the corresponding frustrated Heisenberg model spontaneously breaks time-reversal or parity symmetries.

Of course, a continuous family of *models* does not ensure that the corresponding *states* will vary smoothly, since a phase transition could (and frequently will) intervene. A necessary condition for the absence of a phase transition between the large and small-U limits is that both limiting states must have the same symmetry (no-crossing rule). For example, weakly frustrated square-lattice antiferromagnets are thought to have Néel-ordered[11–13] ground states, so one cannot expect the (paramagnetic) ground states of tight-binding models (2) with weak second-neighbor hopping to continue smoothly as U is increased. A second requirement for continuity between a small-U state and a Mott insulator is that the small-U state must be locally neutral with a gap in the charged excitation spectrum (insulator rule). This condition ensures

that a metal-insulator transition does not interrupt the continuation process.

Which link phases ϕ_{ij} are most likely to permit continuation from a (paramagnetic) Slater determinant to a translationally invariant Mott insulator? The similarity between the generalized Hubbard model (2) and the mean-field theory (1) suggests distributions of flux which correspond to mean-field solutions with uniform magnitudes $|\chi_{ij}|$. The corresponding Slater determinant will then have spin-correlations which should closely resemble its large-U cousin, facilitating a smooth interpolation between the two states. It is also necessary to have a single-particle gap at $U = 0^+$, to satisfy the insulator rule. To obtain a translationally invariant insulator the charge density must also be uniform and the current on each link must vanish. This latter condition is simply the statement that the expectation value of the Hamiltonian is stationary with respect to varying the link phases, which is automatically satisfied by choosing fluxes corresponding to a uniform-amplitude mean-field state.

A strong candidate for adiabatic continuation (from a tight-binding model to a spin-liquid) in the strongly frustrated regime is then the chiral Hubbard model[3,8] with $\pi/2$ flux per triangle. It has a spin-singlet translationally invariant ground state that breaks time-reversal and parity (satisfying the no-crossing rule) and the presence of π flux per plaquette doubles the (magnetic) unit cell opening a "chiral gap" to single-particle excitations for nonzero next-nearest-neighbor hopping (satisfying the insulator rule).

I(c) **Exact Diagonalization of a Periodic Small-Cluster Hamiltonian.** The approach used in this contribution is the small-cluster approximation[14] which consists in the exact diagonalization of the generalized Hubbard Hamiltonians (2) applied to a small cluster with periodic boundary conditions (PBC). The small-cluster approach begins with the periodic crystal approximation,[15] modeling a bulk crystal by a lattice of M sites with PBC. Standard approaches[16] take the thermodynamic limit ($M \rightarrow \infty$) of

the noninteracting system (sampling a continuum in momentum space that spans the Brillouin zone) and treat the subsequent electron-correlation effects in an approximate manner. The small-cluster approach fixes the number of lattice sites to be small (restricting the momentum-space sampling to a coarse grid of high-symmetry points) but solves *exactly* for all electron-correlation effects. The one-electron band structure of both methods is identical at the sampled wavevectors. The relationship of the many-body solutions (at equal electron concentration) for the macroscopic crystal and the small cluster is much more complicated because of uncontrolled finite-size effects in the latter. However, the small-cluster approach provides a rigorous and complimentary method to study the many-body problem that may be extrapolated to macroscopic crystals.

The small-cluster approach was proposed independently for the Hubbard model by Harris and Lange[17] and Falicov and Harris[18] with the exact solution of the two-site cluster. The solution of the four-site square (and tetrahedral) cluster[19] marked the first time that group theory was used to factorize the Hamiltonian (2) into block-diagonal form by using basis functions of definite spin that transform according to the irreducible representations of the full space group. Recent work has concentrated on moderately sized ($M \leq 20$) square-lattice clusters[20,21]. A brief history of applications of the small-cluster approach to different geometries and real materials can be found in Ref. 21.

This contribution examines the ground-state symmetry, wavevector, spin, and correlation functions for the ordinary and the chiral Hubbard models at half-filling on an eight-site square-lattice cluster as functions of the interaction strength U and of the hopping parameters t and t'. Section II discusses the symmetries of the two models and the method of calculation; Section III includes the results for the ground states of both models and their properties; the final section presents the conclusions and suggestions for further work.

II. Symmetries and Calculational Methods

Two different eight-site square-lattice clusters are illustrated in real and reciprocal space in Figs. 1 and 2: the "ordinary" Hubbard model[22] and the "chiral" Hubbard model[3,8]. Both models have hopping amplitudes with the same *magnitudes* for the nearest-neighbor hopping (t) and for the next-nearest-neighbor hopping (t'), respectively, but differ in the relative phases of the hopping parameters. The Hubbard model has all real hopping matrix elements whereas the chiral Hubbard model has relative phases chosen so that each fundamental triangle contains a "flux" of $\pi/2$ (in units where one flux quantum = 2π). Tables I and II summarize the nonzero hopping matrix elements t_{ij} for the two models in terms of the parameters t and t'. One should note that the factor of two multiplying the next-nearest-neighbor hopping matrix elements arises from a renormalization of the hopping parameters caused by the PBC (the four next-nearest-neighbors of an odd [even] site i are *two* each of the remaining odd [even] sites except for the site $i \pm 4$).

(i) **Number operator.** The total-number operator for each spin $N_\sigma = \sum_i n_{i\sigma}$ commutes with the Hamiltonian in equation (2) and is a conserved quantity. The many-body states may be labeled by the total number of electrons $N = N_\uparrow + N_\downarrow$.

(ii) **Spin symmetry.** The total z-component of spin $S_z = \frac{1}{2}(N_\uparrow - N_\downarrow)$, formed from the *difference* of these number operators, is the third component of an internal SU(2) spin symmetry with raising and lowering operators, $S_+ = \sum_i c_{i\uparrow}^\dagger c_{i\downarrow}$ and $S_- = (S_+)^\dagger$, that commute with the Hamiltonian (2)

$$[S_+, S_-] = 2S_z \quad , \quad [S_z, S_\pm] = \pm S_\pm \quad , \quad [H, S_\pm] = [H, S_z] = 0 \quad . \qquad (4)$$

These commutation relations imply that the square of the total-spin operator $S^2 = \frac{1}{2}(S_+ S_- + S_- S_+) + S_z^2$ also commutes with the Hamiltonian, so the many-body

states may be labeled by their total spin S and total z-component of spin m_S, with every state in a given spin multiplet degenerate in energy.

(iii) **Pseudospin symmetry.** Another internal SU(2) "pseudospin" symmetry can be found in special cases.[23–25] The z-component of pseudospin is given by $J_z = \frac{1}{2}(N - M)$. As seen above it commutes with the Hamiltonian; it also satisfies an SU(2) algebra

$$[J_+, J_-] = 2J_z \quad , \quad [J_z, J_\pm] = \pm J_\pm \quad , \tag{5}$$

with the pseudospin raising and lowering operators: $J_+ = \sum_j \exp(i\theta_j) c_j^\dagger{}_\downarrow c_j^\dagger{}_\uparrow$ and $J_- = (J_+)^\dagger$. Although the latter do not commute with the Hamiltonian, they become raising and lowering operators of the Hamiltonian,

$$[H, J_\pm] = \pm U J_\pm \quad , \tag{6}$$

whenever the phase condition

$$t_{ij} = -e^{i(\theta_i - \theta_j)} t_{ij}^* \quad , \tag{7a}$$

is satisfied, or equivalently

$$\theta_i - \theta_j \equiv 2\phi_{ij} + \pi \pmod{2\pi} \tag{7b}$$

is satisfied. If (6) holds, then the square of the pseudospin operator $J^2 = \frac{1}{2}(J_+ J_- + J_- J_+) + J_z^2$ commutes with the Hamiltonian and is another conserved quantity. The phase condition can be satisfied whenever the hopping matrix is bipartite (*i.e.*, when there are two disjoint sublattices A and B with nonzero hopping between $A \longleftrightarrow B$ only) by the choice

$$\theta_i = \begin{cases} 0 , & i \in A \\ \pi , & i \in B \end{cases} ; \tag{8}$$

Equation (7) holds for the ordinary Hubbard model when $t' = 0$, but cannot be

satisfied otherwise. The phase condition (with the phase choice of Eq. 8) is always satisfied for the chiral Hubbard model when one chooses a gauge that is real for $A \longleftrightarrow B$ sublattice hopping, and imaginary for $A \longleftrightarrow A$ and $B \longleftrightarrow B$ sublattice hopping. The many-body states for the half-filled band ($N = M$) all have $J_z = 0$. In the case of the chiral Hubbard model they may also be labeled by their pseudospin J.

(iv) **Space operations for the ordinary Hubbard model.** The space group of the ordinary Hubbard model is a symmorphic, moderately sized finite group constructed from the C_{4v} point-group operations and the eight translation vectors of the lattice: the four nearest-neighbor translations are denoted by τ; the two next-nearest-neighbor translations by θ; and the one third-nearest-neighbor translation by Ω. The space group is of order 64 and is composed of 16 classes. The Brillouin zone[26] (see Fig. 1) is sampled at four symmetry stars: Γ (d=1); M (d=1); X (d=2); and Σ (d=4). The character table[26] is reproduced in Table III.

(v) **Site-permutation operations for the ordinary Hubbard model.** There is a larger group, a cluster-permutation group, that includes the space group as a subgroup and is generated by the space-group generators plus a permutation operator that commutes with the Hamiltonian but is not a space-group operation.[27] In general, this extra permutation operator may be constructed from a set of transpositions (pair interchanges): the origin is interchanged with the site that is farthest away from it. The remaining sites are also pairwise interchanged (if necessary) so that the original neighbor structure of the cluster is preserved. The resultant permutation operator is a nonrigid mapping of the lattice onto itself and, therefore, is not an element of the space group. For example, the nearest-neighbors of site-1 are the sites 2, 4, 6, and 8 (see Fig. 1) and the next-nearest-neighbors are the sites 3 and 7. Site-5 has an *identical* neighbor structure, so the permutation operator P that interchanges site-1 and site-5

will commute with the Hamiltonian but it is *not* simply a combination of translations and point-group operations and hence is not a space-group operation. A similar permutation operator has been found for other clusters, *e.g.* a ten-site square-lattice cluster.[27] The existence of this nontrivial permutation operator is a *finite-size effect* of periodic clusters since an infinite system does not have any symmetry beyond that of the space group. It also depends strongly on the geometry of the system since every finite cluster does not necessarily have this extra "hidden" symmetry.

The cluster-permutation group is composed of 128 elements divided into twenty classes and recorded in Table IV. Note that the presence of the permutation operator P forces physically different space-group operations (such as the translations, rotations and reflections) to be sometimes in the same class. The character table is reproduced in Table V and includes the compatibility relations between representations of the cluster-permutation group and the real space-group in the last column.

The group of translations forms an abelian subgroup of the cluster-permutation group, but it is not an invariant subgroup. This means that one cannot build representations of the cluster-permutation group in the ordinary manner[28] for a space group and, in particular, there are some representations that require essential degeneracies between states that have different wavevectors. Such is the case for representations ϕ_1, ϕ_2, ϕ_3, and ϕ_4 in Table V.

(vi) **Space operations for the chiral Hubbard model.** The fixing of gauge for the chiral Hubbard model drastically reduces the symmetry of the Hamiltonian. The crystal structure becomes a rectangular lattice with a basis of two atoms (see Fig. 2); there are no fourfold rotations or mirror planes. The space group is a symmorphic group constructed from the C_2 point-group operations and the four translation vectors of the lattice. It is of order 8 and composed of 5 classes. The Brillouin zone[26] (see Fig. 2) is sampled at three symmetry stars: Γ (d=1); X (d=1); and Σ (d=2). The

character table[26] is reproduced in Table VI.

There are no finite-size-effect permutation operators that commute with the Hamiltonian for the chiral Hubbard model. This is because the preservation of the neighbor structure of the cluster is not a sufficient condition for a permutation operator to commute with the Hamiltonian if the phases in the hopping matrix are not uniform.

(vii) **Gauge-space operations for the chiral Hubbard model.** There is a larger group, a "gauge-space" group, that includes the space group as a subgroup and is composed of rotations and translations followed by gauge transformations. The gauge transformations χ are unitary operators of order 2 (*i.e.*, square to the identity); they are composed of products of the single-site gauge transformations

$$G_i \equiv (1-2n_{i\uparrow})\,(1-2n_{i\downarrow}) \quad , \; G_i^{\dagger} = G_i^{-1} = G_i \quad , \; G_i^{2} = 1 \quad , \tag{9}$$

which change the *sign* of the electron creation and annihilation operators

$$G_i\, c_{j\sigma}^{\dagger}\, G_i = (-1)^{\delta_{ij}}\, c_{j\sigma}^{\dagger} \quad , \; G_i\, c_{j\sigma} G_i = (-1)^{\delta_{ij}}\, c_{j\sigma} \quad , \tag{10}$$

at the corresponding atomic site. The uniform gauge transformation $\bar{E}$

$$\bar{E} = \prod_{i=1}^{8} G_i \tag{11}$$

changes the sign of the creation and annihilation operators at every site and, acting on state vectors, equals 1 [-1] when the number of electrons is even [odd]. The full group, which allows $\bar{E}$ to be 1 or [-1], is discussed in the appendix. The case with

$\bar{E} = 1$ is discussed here since the half-filled band contains an even number ($N = 8$) of electrons. In this case, the gauge-space group requires three nontrivial gauge transformations

$$\chi_1 = G_3 G_7 \quad , \; \chi_2 = G_4 G_8 \quad , \; \chi_3 = G_1 G_4 G_5 G_8 \quad , \tag{12}$$

in its group elements. The group is generated by a fourfold rotation followed by a gauge transformation (gauge-rotation) — $\chi_1\{C_4|0\}$, the translation from site-1 to site-2 — $\{E|\tau_2\}$, and a translation from site-1 to site-4 followed by a gauge transformation (gauge-translation) — $\chi_3\{E|\tau_4\}$. The gauge-space group, which commutes with the chiral Hubbard model Hamiltonian, is composed of 32 elements divided into 11 classes and recorded in Table VII. The character table is reproduced in Table VIII.

The group of translations and gauge-translations forms an abelian invariant subgroup of the gauge-space group; therefore Bloch's theorem[29] holds with gauge–wavevectors[30] distributed in a gauge-Brillouin zone (see Fig. 2). The gauge-Brillouin zone is sampled at four symmetry stars: γ (d=1); m (d=1); x (d=2); and σ (d=4). Lower-case letters are used to denote the gauge-wavevectors; the compatibility relations between representations of the gauge-space group and the real space group have been included in the last column of Table VI. The gauge-space group is *isomorphic* to the space group of an eight-site square lattice with point group C_4, which is physically sensible since the "magnetic field" is uniform.

(viii) **Particle-hole parity operator.** A particle-hole parity operator[23,31]

$$R = G_1 G_3 G_5 G_7 \prod_{i=1}^{8} (c_i^{\dagger}{}_{\uparrow} + c_{i\uparrow})\,(c_i^{\dagger}{}_{\downarrow} + c_{i\downarrow}) \tag{13}$$

is constructed out of the B-sublattice gauge transformation and the operator that interchanges particles with holes. The particle-hole parity operator is unitary and squares to one so its eigenvalues are ± 1. It satisfies a commutation relation with the Hamiltonian (2)

$$[H\,,R] = 2U\,J_z\,R \tag{14}$$

whenever the hopping matrix t_{ij} obeys

$$t_{ij} = t_{ji} \quad \text{for } i \in A\,,\, j \in B \quad \text{or } i \in B\,,\, j \in A \quad ;$$

$$t_{ij} = -t_{ji} \quad \text{for } i \in A\,,\, j \in A \quad \text{or } i \in B\,,\, j \in B \quad . \tag{15}$$

The particle-hole parity operator commutes with the Hamiltonian if condition (15) is satisfied and $J_z = 0$ (half-filled band). Condition (15) holds for the ordinary Hubbard model only when $t' = 0$ but always holds for the chiral Hubbard model (with the chosen gauge). The particle-hole parity operator anticommutes with the z-component of spin $\{R\,, S_z\}_+ = 0$ so it may be used as an additional symmetry label for the many-body states of the chiral Hubbard model with $m_S = 0$.

An interesting characteristic of the chiral Hubbard model is that it retains all of the "special" parameter-independent symmetries (pseudospin and particle-hole parity) of the nearest-neighbor Hubbard model on a bipartite lattice even when next-nearest-neighbor hopping introduces frustration. The chiral Hubbard model also does not have the finite-size effect of extra permutation symmetries that are not space-group (gauge-space-group) symmetries.

(ix) **Parameter-dependent symmetries.** In addition to the parameter-*independent* symmetries there are two classes of parameter-*dependent* symmetries. The first class is geometrical and depends on the ratio t'/t. When $t'/t = 0$, the Hubbard model on an eight-site square-lattice cluster is *identical* to the Hubbard model on an eight-site body-centered-cubic-lattice cluster.[21] When $t'/t = 1/2$, the renormalized hopping to nearest-neighbors equals the renormalized hopping to next-nearest-neighbors and the eight-site square-lattice cluster becomes an eight-site triangular-lattice cluster which is, in turn, *identical* to an eight-site face-centered-cubic-lattice cluster. In this second case, the large U solutions are known to be threefold degenerate at half–filling.[13,21] There are no geometrical degeneracies for the chiral Hubbard model because the hopping matrix elements have nonzero phases.

The second class is dynamical and depends on the interaction parameter U. The first two of an infinite class of conserved currents have already been found[32,33] for the

nearest-neighbor Hubbard model in one-dimension. Almost certainly additional currents exist for finite clusters since any finite cluster can be mapped onto a one-dimensional ring with hopping terms that extend beyond nearest-neighbors, but these currents have not been determined for either of the models considered here.

(x) **Simultaneous-eigenvector symmetry.** Finally, there is a whole class of eigenstates of the Hamiltonian (2) whose structure (although not necessarily their energies) is independent[23,25] of the interaction parameter U. This occurs whenever an eigenstate of the kinetic energy is *simultaneously* an eigenstate of the interaction term. An example is the fully polarized ferromagnetic state which is annihilated by both the kinetic and potential energy operators. Such phenomenon does not often occur and it is not pursued further here.

The total number of independent many-body states for the half-filled band of an eight-site cluster is 12,870. The systematic application of group theory is used to reduce the size of the Hamiltonian matrix. The grand orthogonality theorem and the matrix-element theorem[34–36] (generalized Unsöld theorem) guarantee that the Hamiltonian matrix will be in block-diagonal form, with no mixing between states of different spin or spatial symmetry, when it is expanded in a symmetrized basis that has definite spin and transforms according to the (1,1) matrix elements of an irreducible representation of the symmetry group. Neither the additional pseudospin, nor the particle-hole parity symmetries (which produce a further reduction of the block sizes for the chiral Hubbard model), nor any of the parameter-dependent symmetries were utilized. Use was made of a symmetry-adapted computer algorithm[21] that calculates the (1,1) matrix elements[37] of the irreducible representations, constructs projection operators from these matrix elements, and operates on maximum z-component of spin states ($m_S = S$) to generate symmetrized basis functions of definite spin and spatial symmetry. The Hamiltonian blocks are determined *exactly* in this symmetrized basis

(incorporating multiple-precision integer arithmetic[38] when necessary) and are checked for completeness within each subspace of definite spin and spatial symmetry. The resultant blocks are diagonalized by the so-called QL algorithm[39] (which determines all of the eigenvalues and eigenvectors) when the blocks were smaller than 100×100 and by Cullum and Willoughby's single-vector Lanczos routines[40] (which determine the lowest five eigenvalues and eigenvectors) for the larger blocks. Tables IX and X summarize the reduced block sizes for the ordinary Hubbard model and for the chiral Hubbard model. The application of group theory reduces the block sizes by a factor of 50 which, in turn, reduces the diagonalization time by five orders of magnitude.

III. Results

The spectrum of a generalized Hubbard Hamiltonian (2) is independent[23,41] of the sign of t or t' for the half-filled band, so only the cases with $t \geq 0$ and $t' \geq 0$ were considered. In the strong-interaction limit ($U \rightarrow \infty$), both the Hubbard model and the chiral Hubbard model approach the same frustrated Heisenberg antiferromagnet[10,17,42] with exchange integrals $J = 4t^2/U$ (nearest-neighbor) and $J' = 4t'^2/U$ (next-nearest-neighbor). Therefore, the ground-state phase diagrams for both models are expected to be identical to second order $O(t^2/U)$ although at higher order they need not be the same. It is known[9] that the ground state of the nearest-neighbor Hubbard model ($t' = 0$) is a spatially uniform spin-singlet that may be adiabatically continued from a spin-density wave insulator ($U = 0^+$) to a two-sublattice Néel antiferromagnet[11] ($U \rightarrow \infty$) without level crossings. The eight-site frustrated Heisenberg model has been studied for all values of J and J' in Ref. 13. It undergoes a level crossing from a two-sublattice Néel AF to a four-sublattice Néel AF, with a threefold degeneracy at the level crossing as J'/J increases.

There are four different ground-state correlation functions that were computed in order to determine the ground-state properties: The spin-spin correlation function (L_i);

the z-component of spin-z-component of spin correlation function (M_i); the number-number correlation function (N_i); and the spin-triple-product correlation function (O_{124}). The correlation functions are defined by the following ground-state expectation values:

$$L_i = \frac{1}{\nu_i} \sum_{(jk)=i\text{th NN}} <GS|\mathbf{S}_j \cdot \mathbf{S}_k|GS> \quad , \quad i = 0,1,2,3 \quad ; \tag{16a}$$

$$M_i = \frac{1}{\nu_i} \sum_{(jk)=i\text{th NN}} <GS|S_j^z S_k^z|GS> \quad , \quad i = 0,1,2,3 \quad ; \tag{16b}$$

$$N_i = \frac{1}{\nu_i} \sum_{(jk)=i\text{th NN}} <GS|n_j\, n_k|GS> \quad , \quad i = 0,1,2,3 \quad ; \tag{16c}$$

$$O_{124} = <GS|\mathbf{S}_1 \cdot \mathbf{S}_2 \times \mathbf{S}_4|GS> \quad ; \tag{16d}$$

where i denotes the distance between site-j and site-k and ν_i denotes the number of site-pairs separated by this distance. The correlation functions satisfy three sum rules:

$$\sum_{i=0}^{3} \nu_i L_i = S(S+1) \quad ;$$

$$\sum_{i=0}^{3} \nu_i M_i = m_S^2 \quad ;$$

$$\sum_{i=0}^{3} \nu_i N_i = N^2 = 64 \quad ; \tag{17}$$

since the ground state has definite total-spin and definite electron number. Furthermore, the spin correlation functions are related by

$$L_i = 3M_i \quad , \quad \text{for } S = 0 \quad , \tag{18}$$

i.e., whenever the ground state is a spin-singlet. The sum rules (17) and the relation (18) hold for all the correlation functions that were calculated. The spin-triple-product correlation function is formed from three spins that lie on the vertices of a right triangle consisting of two nearest-neighbor pairs and one next-nearest-neighbor pair. This is the only (potentially) nonzero spin-triple-product correlation function for an eight-

site cluster.

The maximum hopping integral $T = max(t, t')$ was chosen as the unit of energy and the hopping parameters were selected in the range

$$0 \leq \frac{2t'}{t+2t'} \leq 1 \quad , \tag{19}$$

from pure nearest-neighbor hopping ($t' = 0$) to pure next-nearest-neighbor hopping ($t = 0$). The interaction strength was varied in the range

$$0 \leq \frac{U}{4t+4t'+U} \leq 1 \quad , \tag{20}$$

from the noninteracting regime ($U = 0$) to the strong-coupling limit ($U = \infty$).

(i) **Ordinary Hubbard Model.** The one-electron band structure of the Hubbard model consists of four levels: Γ_{1p} (degeneracy d=1; energy $\varepsilon = -4t - 4t'$); Σ_{1p} (d=4; $\varepsilon=0$); X_{1p} (d=2; $\varepsilon=4t'$); and M_{1p} (d=1; $\varepsilon=4t-4t'$). The ground state for the noninteracting ($U = 0$) half-filled band is formed by filling the Γ_{1p} level and placing six electrons in the Σ_{1p} level for $t' < t$ or by filling the Γ_{1p} and M_{1p} levels and placing four electrons in the Σ_{1p} level for $t' > t$. In either case, the noninteracting half-filled band has a degenerate ground state and would require degenerate perturbation theory to determine the small-U ground state.

The symmetry of the ground state is recorded by attaching the spin multiplicity ($2S+1$) as a superscript to the symbol for the irreducible representation that transforms according to the many-body state (as given in Table V). The ground-state symmetries are plotted as a function of the relative hopping (19) along the vertical axis and of the interaction strength (20) along the horizontal-axis in the phase diagram of Figure 3. The spin-spin correlation functions (L_i) and the number-number correlation functions (N_i) are recorded in Fig. 4 and Fig. 5 respectively, for three different values of t'/t. There are no discontinuities in the correlation functions when there are no level

crossings in the ground state. Note that as $U \to \infty$ the ground state contains one electron per site and the spins are oriented[13] into a two-sublattice Néel AF ($t' < t/2$) or a four-sublattice Néel AF ($t' > t/2$). The spin-triple-product correlation function, O_{124}, vanishes for all values of t, t', and U (since the ground states are invariant under parity).

Note that the presence of the cluster-permutation group symmetries ϕ_2 and ϕ_4 as ground states is a finite-size effect that requires particular states with wavevectors Γ and M, or M and X, to be "accidentally" degenerate.

There are only two regimes where the ground state may be adiabatically continued from $U = 0^+$ to $U \to \infty$ at fixed t'/t without any level crossings. At $t' = 0$ the ground state has ${}^1\Gamma_{1n}$ symmetry and continuously changes[9] from a spin-density wave insulator ($U = 0^+$) to a two-sublattice Néel AF ($U \to \infty$). If $t' > t$, the ground state also has ${}^1\Gamma_{1n}$ symmetry and continuously changes from another spin-density wave insulator ($U = 0^+$) to a four-sublattice Néel AF ($U \to \infty$). For any other value of t', $0 < t' < t$, there are level crossings as U increases from zero to infinity.

There is a small region of phase space ($t \approx t' \approx U$) where the ground state is *ferrimagnetic* (symmetry ${}^5\Sigma_{2n}$). This region is very sensitive to the ratio of the hopping parameters t'/t but is stable for a wide range of the interaction strength, producing the sliver in Fig. 3. The nonzero magnetic moment of this state arises from a complicated interaction between spin and orbital angular momentum that becomes favorable when the two hopping parameters and the interaction strength are all of the same order of magnitude. This mechanism for producing ferrimagnetism in a half-filled band is different from Lieb's mechanism,[43] since the hopping matrix makes the lattice *not* bipartite. It is similar in the sense that the magnetism is not saturated. To the authors' knowledge, this is the first observation of a *nonzero* magnetic moment in the square-lattice Hubbard model at half-filling.

When $t' = t/2$ the square-lattice cluster becomes a face-centered-cubic-lattice cluster and the ground state has extra degeneracies. The thick-dashed line in Fig. 3 corresponds to a ground state with symmetry ${}^1\phi_2 \oplus {}^1\phi_4$ ($d = 6$) that separates the region where the ordering of the small U ground state changes. The chain-dashed line corresponds, for large-U, to the threefold degenerate state ${}^1\Gamma_{1n} \oplus {}^1\Gamma_{1n} \oplus {}^1\Gamma_{3n}$, and shows that the ordinary Hubbard model ground state is threefold degenerate in the limit $U \rightarrow \infty$ to all orders in $|t|$.

A few cases of accidental degeneracies remain in the many-body spectrum.[44] Heilmann's numerical methods[45] were used to search for parameter-independent hidden symmetries that explain these accidental degeneracies but the problem was not completely resolved.[46]

(ii) **Chiral Hubbard Model.** The one-electron band structure for the chiral Hubbard model (see the Appendix) consists of four twofold degenerate levels: ω_1 (energy $\varepsilon = -\sqrt{8}\,t$); ω_2 ($\varepsilon = \sqrt{8}\,t$); ω_5 ($\varepsilon = 4t'$); and ω_6 ($\varepsilon = -4t'$). The noninteracting ground state ($U = 0$) for the half-filled band is formed by completely filling the lowest two energy levels. It is nondegenerate with symmetry ${}^1\gamma_2$ (see Table VIII) for all cases except $t = 0$ or $t' = 0$, where the ground state is degenerate. The large U ground state is known[13,21] to have symmetry ${}^1\gamma_1$ everywhere except at the point $t' = t/2$ where the ($U \rightarrow \infty$) ground state is threefold degenerate (${}^1\gamma_1 \oplus {}^1\gamma_1 \oplus {}^1\gamma_2$). Therefore, the chiral Hubbard model may satisfy the no-crossing rule only at three points: $t = 0$; $t' = t/2$; and $t' = 0$.

The ground-state symmetries are plotted as a function of the relative hopping (19) along the vertical axis and of the interaction strength (20) along the horizontal axis in the phase diagram of Fig. 6. The ground state is always a spin singlet ($S = 0$), a pseudospin singlet ($J = 0$), and has even particle-hole parity ($R = 1$). The spin-spin correlation functions (L_i), the number-number correlation functions (N_i), and the spin-triple-product correlation functions (O_{124}) are recorded in Fig. 7, Fig. 8, and Fig. 9

respectively, for representative values of t'/t. As $U \rightarrow \infty$ the ground state contains one electron per site and is oriented[13] in a two-sublattice Néel AF ($t' < t/2$) or a four-sublattice Néel AF ($t' > t/2$) as expected. The case with $t' = t/2$ (Fig. 7) is not ordered as a Néel AF, but rather has intermediate-range AF order that may be interpreted as the approximation to a spin–liquid[1–3] for a finite system. The spin-triple-product correlation function does not vanish for the chiral Hubbard model (at finite U) because of the explicit breaking of time-reversal and parity symmetries in the Hamiltonian (see Table II). The sign of O_{124} changes at the level crossing between the ${}^1\gamma_2$ (small U) and the ${}^1\gamma_1$ (large U) ground state and its magnitude approaches zero.

It is interesting to note that, as U approaches infinity (at constant t and t') not only is $O_{124} \rightarrow 0$ but, in addition, the derivative of O_{124} with respect to $(1/U)$ also approaches zero (except for the case with $t' = t/2$). This feature could be understood in terms of a "triple-product" susceptibility if the following facts are taken into account:

1) The derivative of O_{124} with respect to $(1/U)$ is directly proportional to the expectation value for the ground state for $U \rightarrow \infty$ of

$$\left[\sum_{<i,j,k>} \mathbf{S}_i \cdot \mathbf{S}_j \times \mathbf{S}_k \right]^2 \quad ; \tag{21}$$

2) In the cluster examined here all eigenstates in the $U \rightarrow \infty$ limit are independent[13] of t and t';

3) The eigenstates of the Hamiltonian either for $t = 0$ or for $t' = 0$ are eigenstates of $\mathbf{S}_1 \cdot \mathbf{S}_2 \times \mathbf{S}_4$, with zero eigenvalue because of the conserved chiral symmetry;

4) From 1), 2), and 3) it follows that the expectation value of (21) is zero, regardless of the values of t and t'. Therefore the value of the derivative of O_{124} with respect to $(1/U)$ as $U \rightarrow \infty$ must be identically zero for these cases.

It is important to emphasize that the property 2) above is probably a consequence of the finite cluster Hamiltonian, and in all probability does not survive for arbitrary Hamiltonians in the thermodynamic limit.

The specific value $t' = t/2$ is singular. The derivative mentioned above is zero if the limit $U \to \infty$ is taken before $t' \to t/2$; the slope is finite if the limits are taken in the opposite order (see Fig. 9). In the latter case condition 3) is violated (the ground state of the Hamiltonian is *not* an eigenstate of $\mathbf{S}_1 \cdot \mathbf{S}_2 \times \mathbf{S}_4$).

There are three points where the ground state may be adiabatically continued (at fixed t'/t) from $U = 0^+$ to $U \to \infty$ without any level crossings: at $t = 0$; at $t' = t/2$; and at $t' = 0$. The two cases when one of the hopping parameters vanishes produce the smooth crossover from a flux-phase spin-density-wave limit ($U = 0^+$) to a quantum Néel limit ($U \to \infty$) as suggested[47] by Hsu. The other case ($t' = t/2$) indicates that the $U = 0$ ground state of a tight-binding model *can* be smoothly related to the ground state of a frustrated Heisenberg model with no intervening phase transition.

On a 4×4 cluster,[13] the ground state of the frustrated Heisenberg model remains nondegenerate, although there is a sharp level repulsion in the vicinity of the transition between the two- to four-sublattice Néel states. There is as yet no evidence which points to the existence of a "spin-liquid" phase in any finite system calculation.

There are a few interesting results for the excited states in the chiral Hubbard model. The particle-hole parity operator is not an independent quantity, but rather satisfies $R = (-1)^{S+J}$ for all cases tested. A few accidental degeneracies remain in the many-body spectrum: Fifteen cases arise from many-body eigenstates that are simultaneous eigenvectors[48] of the kinetic energy and potential energy operators of (2); and eight levels of ${}^1\gamma_3$ ($J = 0$) symmetry are degenerate with eight levels of ${}^1\gamma_4$ ($J = 0$) symmetry. Heilmann's method[45] is used to show that the latter degeneracies do not correspond to any parameter-independent symmetries, so they probably arise from the dynamical effect[49] discussed in Ref. 33.

IV. Conclusions

Exact solutions of the Hubbard model on an eight-site square lattice cluster with nearest- and next-nearest-neighbor hopping t and t' have been presented for two different flux distributions. In the first case (the "ordinary" Hubbard model), the flux through any closed loop vanishes, and all link phases ϕ_{ij} can be set to zero. In the second case (the "chiral" Hubbard model), the link phases are selected so that the flux through every elementary triangle is $\pi/2$. The ground and low-lying states of an eight site cluster with PBC are exactly solved for both the ordinary Hubbard model (Fig. 1) with nearest- and next-nearest-neighbor hopping and the chiral Hubbard model (Fig. 2) with nearest- and next-nearest-neighbor hopping in the presence of a "magnetic field" which couples only to orbital motion and whose strength corresponds to one-half flux quantum per plaquette. These exact solutions are made possible by using the cluster-symmetry group of the models and spin-rotation symmetry. In the case of the ordinary Hubbard model, the cluster-symmetry group includes the space group and extra site-permutation operators (which are a finite-size effect of the eight-site square-lattice cluster). In the case of the chiral Hubbard model, the complete cluster-symmetry group is composed of combinations of gauge transformations and space-group operations.

The phase diagram of the half-filled ordinary Hubbard model (with zero flux through every closed path) is shown in Fig. 3. For small or large t'/t, the ground state of the system is seen to vary smoothly from the $U=0^+$ spin-density-wave limit to the large-U quantum Néel limit, as discussed[9] by Schrieffer, Wen, and Zhang. When both hopping parameters are comparable, however, we find several level crossings between the small and large-U limits, and a complicated set of ground-state phases at small and intermediate U. These intermediate-U phases include a peculiar state which has a nonzero (but unsaturated) magnetic moment, and contradicts the folklore that the ground state of a half-filled Hubbard model is spin quenched. It is found that for $0<t'<t$ there is no path from $U=0^+$ to large U along which the ground state

changes continuously. Thus when both nearest- and next-nearest-neighbor hopping contribute appreciably to the kinetic energy, one cannot apply a simple weak-coupling theory to extract the physics of the corresponding large-U frustrated Heisenberg spin system. According to Fig. 3, the best path from weak coupling to to the frustrated Heisenberg model either starts with $t' = 0$, proceeds to large-U, and then turns on a finite t', or starts with $t' > t$, proceeds to large-U, and then decreases t' to values $t' < t$.

The phase diagram of the half-filled chiral Hubbard model with a flux of $\pi/2$ per triangle is displayed in Fig 6. When t or t' vanish, there is a smooth transit from the flux-phase spin-density-wave limit to the quantum Néel limit, as suggested[47] by Hsu. When t and t' are comparable, however, the phase diagram acquires a pleasing simplicity when compared with that of the ordinary Hubbard model shown in Fig. 3. A single phase at $t' = t/2$ stretches from the $U = 0$ axis all the way to $U = \infty$, where it pinches off to a single point at the transition between the two-sublattice and the four-sublattice Néel states. In accord with several other calculations, no evidence was found for an intermediate spin-liquid phase (except for a single point) in the spin-1/2 Heisenberg model with nearest- and next-nearest-neighbor antiferromagnetic couplings on the relatively small eight-site cluster. The results do suggest, however, that the ground state of a $U = 0$ tight-binding model (at one value of t'/t) may be smoothly related to the ground state of a frustrated Heisenberg model without an intervening phase transition. It is plausible that exact-diagonalization studies of Heisenberg models on larger clusters would indicate whether this region of analytic continuation becomes finite or disappears entirely by comparing the symmetries of (candidate) $U = 0$ tight-binding ground states to the corresponding frustrated Heisenberg-model ground state.

Acknowledgments

We acknowledge helpful conversations with M. Crescimanno, S. Kivelson, and T. Pang. J.K.F acknowledges the support of the Department of Education. J.K.F. and L.M.F. acknowledge support at the Lawrence Berkeley Laboratory, by the Director, Office of Energy Research, Office of Basic Energy Sciences, Material Sciences Division, U.S. Department of Energy, under contract No. DE-AC03-76SF00098. D.S.R. acknowledges support by the National Science Foundation grant DMR 89-14440 and from the Alfred P. Sloan Foundation.

Appendix: Full Gauge-Space Group

The uniform gauge transformation $\bar{E}$ (Eq. 11) is a unitary operator that corresponds to multiplication of a many-body wavefunction by the overall phase factor $\exp[i\pi(N_\uparrow+N_\downarrow)]$ which yields 1 [-1] for an even [odd] number of electrons. The element $\bar{E}$ also commutes with every element of the gauge-space group in Table VII. The uniform gauge transformation, therefore, has an identical relationship to the gauge-space group (when one considers representations with an even or odd number of electrons) as a rotation by 2π has to ordinary space groups (when one considers representations with integral or half-integral spin[50]).

The introduction of the uniform gauge transformation as an independent group element produces a double group, called the full gauge-space group, that has 64 elements. Six different gauge transformations

$$\chi_1 = G_3 G_7 \quad , \quad \chi_2 = G_4 G_8 \quad , \quad \chi_3 = G_1 G_4 G_5 G_8 \quad , \quad \chi_4 = G_2 G_3 G_6 G_7 \quad ,$$

$$\chi_5 = G_1 G_2 G_3 G_5 G_6 G_7 \quad , \quad \chi_6 = G_1 G_2 G_4 G_5 G_6 G_8 \quad , \qquad \text{(A.1)}$$

are required for closure. There are 19 classes in the double group and three of those classes include barred and unbarred elements (a barred element corresponds to an unbarred element multiplied by $\{\bar{E} \mid 0\}$). The group elements and class structure are

summarized in Table XI. It must be reiterated that the double-group structure of the full gauge-space group *is not related to the total spin of the electrons,* but rather it arises from the transformation properties of the chiral Hubbard model under gauge transformations.

Since some of the classes of the full gauge-space group include both barred and unbarred elements, all of the "double-valued" representations are at least twofold degenerate, which is analogous to Kramers degeneracy. The eleven "single-valued" representations of the full gauge-space group (which correspond to representations with an *even* number of electrons) can be found in Table VIII. Table XII records the eight "double-valued" representations (which correspond to representations with an *odd* number of electrons) for the full gauge-space group including the compatibility relations with the real space group (Table VI) in the last column.

There is no Brillouin zone or even a gauge-Brillouin zone for the "double-valued" representations because the gauge-translation subgroup (composed of all elements with a point-group operation E or $\bar{E}$) forms a *nonabelian* invariant subgroup of the full gauge-space group: *there is no Bloch's theorem.*

The one-electron band structure of the chiral Hubbard model is easily determined. There are four twofold degenerate levels of symmetries ω_1 (energy $\varepsilon = -\sqrt{8}\,t$), ω_2 ($\varepsilon = \sqrt{8}\,t$), ω_5 ($\varepsilon = 4\,t'$), and ω_6 ($\varepsilon = -4\,t'$). The noninteracting ground state for the half-filled band consists of the filled shells of the ω_1 and ω_6 levels, has symmetry ${}^1\gamma_2$, and is nondegenerate (whenever t and t' are both nonzero).

The fact that all representations corresponding to an odd number of electrons are twofold degenerate implies that a symmetry-lowering distortion of the phases in (2), as has been recently proposed[10] for the spinons and holons, would be energetically more favorable than the "uniform" choice of the chiral Hubbard model.

References

1 P.W. Anderson, Science **235,** 1196 (1987).

2 S. Kivelson, D.S. Rokhsar, and J.P. Sethna, Phys. Rev. B **35,** 8865 (1987).

3 V. Kalmeyer and R.B. Laughlin, Phys. Rev. Lett. **59,** 2095 (1987); R.B. Laughlin, Science **242,** 525 (1988).

4 I. Affleck and J.B. Marston, Phys. Rev. B **37,** 3774 (1988); J.B. Marston and I. Affleck, *ibid.* B **39,** 11538 (1989).

5 G. Baskaran and P.W. Anderson, Phys. Rev. B **37,** 580 (1989).

6 D.S. Rokhsar, Phys. Rev. B **42,** 2526 (1990).

7 C. Gros, Phys. Rev. B **38,** 931 (1988).

8 X.G. Wen, F. Wilczek, and A. Zee, Phys. Rev. B **39,** 11413 (1989).

9 J.R. Schrieffer, X.G. Wen and S.-C. Zhang, Phys. Rev. B **39,** 11663 (1988).

10 D.S. Rokhsar, Phys. Rev. Lett. **65,** 1506 (1990).

11 A Néel antiferromagnet is the quantum-mechanical ground state of an unfrustrated Heisenberg model and can be viewed as a classical Néel state with quantum fluctuations.

12 Numerical studies of frustrated spin-1/2 Heisenberg models suggest that Néel order is destroyed for sufficient frustration, but the nature of the ground states remains unclear. See, *e.g.*, E. Dagotto and A. Moreo, Phys. Rev. B **39,** 4744 (1989) and Ref. 13.

13 F. Figuerido, A. Karlhede, S. Kivelson, S. Sondhi, M. Rocek, and D.S. Rokhsar, Phys. Rev. B **41,** 4619 (1990).

14 For a review see L.M. Falicov in *Recent Progress in Many-Body Theories* Vol. 1, edited by A.J. Kallio, E. Pajanne, and R.F. Bishop, (Plenum, New York, 1988) p. 275; J. Callaway, Physica B **149,** 17 (1988).

15 L.M. Falicov, *Group Theory and Its Physical Applications,* (University of Chicago Press, Chicago, 1966) p. 144ff.

16 D. Pines, *The Many-Body Problem* (Benjamin/Cummings, Reading, 1962).

17 A.B. Harris and R.V. Lange, Phys. Rev. **157,** 295 (1967).

18 L.M. Falicov and R.A. Harris, J. Chem. Phys. **51,** 3153 (1969).

19 A.M. Oleś, B. Oleś, and K.A. Chao, J. Phys. C **13,** L979 (1980); J. Rössler, B. Fernandez, and M. Kiwi, Phys. Rev. B **24,** 5299 (1981); D.J. Newman, K.S. Chan, and B. Ng, J. Phys. Chem. Solids **45,** 643 (1984); L.M. Falicov and R.H. Victora, Phys. Rev. B **30,** 1695 (1984); C.M. Willet and W.-H. Steeb, J. Phys. Soc. Japan **59,** 393 (1990).

20 E. Kaxiras and E. Manousakis, Phys. Rev. B **37,** 656 (1988); E. Kaxiras and E. Manousakis, *ibid.,* **38,** 866 (1988); J. Bonca, P. Prelovsek, and I. Sega, *ibid.,* **39,** 7074 (1989); J.A. Riera and A.P. Young, *ibid.,* **39,** 9697 (1989); *ibid.,* **40,** 5285 (1989); E. Dagotto, A. Moreo, and T. Barnes, *ibid.,* **40,** 6721 (1989); M. Ogata and H. Shiba, J. Phys. Soc. Japan **58,** 2836, (1989); Y. Fang, A.E. Ruckenstein, E. Dagotto, and S. Schmitt-Rink, Phys. Rev. B **40,** 7406 (1989); Y. Hasegawa and D. Poilblanc, *ibid.,* **40,** 9035 (1989); Int. J. Mod. Phys. B **3,** 1853 (1989); A. Parola, S. Sorella, S. Baroni, M. Parrinello, and E. Tosatti, *ibid.,* **3,** 139 (1989); M. Imada and Y. Hatsugai, J. Phys. Soc. Japan **58,** 3752 (1989); D.M. Frenkel, R.J. Gooding, B.I. Shraiman, and E.D. Siggia, *ibid.,* **41,** 350 (1990); E. Dagotto, A. Moreo, R.L. Sugar, and D. Toussaint, Phys. Rev. B **41,** 811 (1990); D. Poilblanc, Y. Hasegawa, and T.M. Rice, *ibid.,* **41,** 1949 (1990); E. Dagotto, A. Moreo, R. Joynt, S. Bacci, and E. Gagliano, *ibid.,* **41,** 2585 (1990); K.-H. Luk and D.L. Cox, *ibid.,* **41,** 4456 (1990); V. Elser, D.A. Huse, B.I. Shraiman, and E.D. Siggia, *ibid.,* **41,** 6715 (1990); D. Poilblanc and Y. Hasegawa, *ibid.,* **41,** 6989 (1990); J. Richter, Z. Phys. B **79,** 403 (1990); I. Sega and P. Prelovsek, Phys. Rev. B **42,** 892 (1990); T. Itoh, M. Arai, and T. Fujiwara, *ibid.,* **42,** 4834

(1990); D. Poilblanc and E. Dagotto *ibid.*, **42,** 4861 (1990); A. Moreo and E. Dagotto, *ibid.*, **42,** 4786 (1990); E. Gagliano, S. Bacci, and E. Dagotto, *ibid.*, **42,** 6222 (1990); G. Fano, F. Ortolani, and A. Parola, *ibid.*, **42,** 6877 (1990).

[21] J.K. Freericks and L.M. Falicov, Phys. Rev. B **42,** 4960 (1990).

[22] J. Hubbard, Proc. R. Soc. London, Ser. A **276,** 238 (1963); *ibid.*, **277,** 237 (1964); *ibid.*, **281,** 401 (1964); *ibid.*, **285,** 542 (1965); *ibid.*, **296,** 82 (1967); *ibid.*, **296,** 100 (1967).

[23] O.J. Heilmann and E.H. Lieb, Trans. NY Acad. Sci. **33,** 116 (1971).

[24] C.N. Yang, Phys. Rev. Lett. **63,** 2144 (1989); M. Pernici, Europhys. Lett. **12,** 75 (1989); S. Zhang, Phys. Rev. Lett. **65,** 120 (1990).

[25] C.N. Yang and S.C. Zhang, Mod. Phys. Lett. A **4,** 759 (1990).

[26] L.P. Bouckaert, R. Smoluchowski, and E. Wigner, Phys. Rev. **50,** 58 (1936).

[27] R. Saito, Sol. St. Commun. **72,** 517 (1989); T. Ishino, R. Saito, and H. Kamimura, J. Phys. Soc. Japan, **59,** 3886 (1990); J.K. Freericks and L.M. Falicov, unpublished.

[28] L.M. Falicov, *Group Theory and Its Physical Applications,* (University of Chicago Press, Chicago, 1966) p. 155ff.

[29] C. Kittel, *Quantum Theory of Solids,* (Wiley, New York, 1987) pp. 179ff.

[30] The labels of the many-body eigenstates are called gauge-wavevectors because they determine the phase shift of these states under normal *and* gauge-translations.

[31] S. Kivelson and W.-K. Wu, Phys. Rev. B **34,** 5423 (1986).

[32] W. Brinkman and T.M. Rice, Phys. Rev. B **2,** 1324 (1970); B.S. Shastry, J. Stat. Phys. **50,** 57 (1988).

[33] H. Grosse, Lett. Math. Phys. **18,** 151 (1989).

[34] M. Tinkham, *Group Theory and Quantum Mechanics,* (McGraw-Hill, New York, 1964) p. 20ff.; p. 80ff.

[35] L.M. Falicov, *Group Theory and Its Physical Applications,* (University of Chicago Press, Chicago, 1966) p. 20ff.; p. 46ff.

[36] A.W. Luehrmann, Adv. in Phys. **17,** 1 (1968).

[37] In the case of representations that have complex-valued (1,1) matrix elements the projection is onto the subspace spanned by the complex representation and its conjugate so that all matrix elements are real.

[38] R.P. Brent, ACM Trans. on Math. Soft. **4,** 57 (1978).

[39] J.H. Wilkinson and C. Reinsch, *Handbook for Automatic Computation, Vol. II: Linear Algebra,* ed. F.L. Bauer, (Springer-Verlag, New York, 1971) p. 227.

[40] J. Cullum and R.A. Willoughby, *Lanczos Algorithms for Large Symmetric Eigenvalue Computations Vol. 1 and 2* (Birkhauser, Basel, 1985).

[41] E.H. Lieb and F.Y. Wu, Phys. Rev. Lett. **20,** 1445 (1968).

[42] P.W. Anderson, Solid State Phys. **14,** 99 (1963); J.R. Schrieffer and P.A. Wolff, Phys. Rev. **149,** 491 (1966); A.H. MacDonald, S.M. Girvin, and D. Yoshioka, Phys. Rev. B **37,** 9753 (1988); A.M. Olés, *ibid.,* **41,** 2562 (1990); A.H. MacDonald, S.M. Girvin, and D. Yoshioka, *ibid.,* **41,** 2565 (1990).

[43] E.H. Lieb, Phys. Rev. Lett. **62,** 1201 (1989).

[44] Two cases have nontrivial energy eigenvalues: nine of the ${}^5\Gamma_{1n}$ levels are degenerate for all values of the interaction strength with nine of the ${}^5M_{1n}$ levels; and nine of the ${}^3\Gamma_{1n}$ levels are degenerate with nine of the ${}^3M_{1n}$ levels. Three cases arise from many-body states that are annihilated by the kinetic energy operator (*i.e.*, they are simultaneous eigenstates of the kinetic and potential energy operators): the level $E = U$ has a degeneracy d = 129; $E = 2U$ has d = 107; and $E = 3U$ has d = 6.

[45] This method uses the fact that the U–independent invariant subspaces of the Hamiltonian correspond to the invariant subspaces of a test matrix that is constructed out of the Hamiltonian (with $U = 1$) and is expressed in a coordinate basis that diagonalizes the Hamiltonian for a particular value of $U \neq 1$. For further details see O.J. Heilmann, J. Math. Phys. **11,** 3317 (1970).

[46] The invariant subspace decomposition produced the trivial one-dimensional subspaces that correspond to each eigenvector that is a simultaneous eigenvector of the two terms in (2) and it produced thirteen nontrivial decompositions in the subspaces highlighted in bold in Table X. The subspace ${}^3M_{1n}$ decomposes into three nontrivial invariant subspaces and the other twelve decompose into two nontrivial invariant subspaces. It is easy to show by a counting argument that the extra symmetry is *not* a permutation symmetry of the eight sites. There are probably two possibilities that can explain the extra symmetry: there may be an extra permutation symmetry of the sixteen orbitals that conserves S^2 and S_z but mixes the space and spin labels creating an even larger group that would explain the accidental degeneracies; there may be an operator similar to the pseudospin J^2 that causes the decomposition and the accidental degeneracies are explained by a dynamical effect using conserved currents as in Ref. 33.

[47] T. Hsu, Phys. Rev. B **41,** 11379, 1990.

[48] A larger number of parameter-independent eigenstates than those constructed in Ref. 25 [out of states that have maximal values of pseudospin $(J = M/2 - S = 4 - S)$] have been found (816 found versus 640 predicted); this disproves Yang and Zhang's conjecture that the only parameter-independent eigenstates are those lying in a maximal-pseudospin family.

[49] The parameter-dependent conserved current would commute with $\{E \mid \tau_2\}$, $\chi_3\{E \mid \tau_4\}$, and R; anticommute with $\chi_1\{C_4 \mid 0\}$; and commute or anticommute with both $SU(2)$ operators. It would take each of the eight eigenstates with ${}^1\gamma_3$

($J=0$) symmetry and map them into the corresponding eigenstate with ${}^1\gamma_4$ ($J=0$) symmetry that has the same energy eigenvalue (and *vice versa*). The other many-body eigenstates would either be annihilated by the current or, if the state is a member of a multiplet (*i.e.*, has symmetry x_1, x_2, or σ_1), it may be mapped into another member of the multiplet by the current.

50 L.M. Falicov, *Group Theory and Its Physical Applications,* (University of Chicago Press, Chicago, 1966) p. 103ff.

Table I. Renormalized hopping matrix elements t_{ij} for $(i < j)$ in the ordinary Hubbard model. The eight cluster sites are illustrated in Fig. 1. All diagonal matrix elements t_{ii} are zero and the matrix elements t_{ij} with $i > j$ are determined by hermiticity $(t_{ij} = t_{ji}^*)$.

parameter	indices $(i\ j)$			
$-t$	(12)	(14)	(16)	(18)
	(23)	(25)	(27)	(34)
	(36)	(38)	(45)	(47)
	(56)	(58)	(67)	(78)
$-2t'$	(13)	(17)	(24)	(28)
	(35)	(46)	(57)	(68)
0	(15)	(26)	(37)	(48)

Table II. Renormalized hopping matrix elements t_{ij} for $(i < j)$ in the chiral Hubbard model. The eight cluster sites are illustrated in Fig. 2. All diagonal matrix elements t_{ii} are zero and the matrix elements t_{ij} with $i > j$ are determined by hermiticity $(t_{ij} = t_{ji}^*)$.

parameter	indices $(i\ j)$			
$-t$	(12)	(14)	(16)	(18)
	(23)	(25)	(27)	(36)
	(45)	(56)	(58)	(67)
t	(34)	(38)	(47)	(78)
$-2it'$	(17)	(28)		
$2it'$	(13)	(24)	(35)	(46)
	(57)	(68)		
0	(15)	(26)	(37)	(48)

Table III. Character table for the space group of the eight-site square-lattice cluster (ordinary Hubbard model). The symbol E is the identity, C_n^m is the rotation by $2\pi m/n$ about the z-axis, σ denotes the mirror planes perpendicular to the $x-$ and $y-$axes and σ' denotes the mirror planes perpendicular to the diagonals $x \pm y$. The translations are denoted by 0 (no translation), τ (nearest-neighbor translation), θ (next-nearest-neighbor), and Ω (third-nearest-neighbor). The subscripts $\parallel$ and $\perp$ refer to translations parallel to or perpendicular to the normals of the mirror planes.

	1	8	2	4	4	4	8	4	4	4	8	2	2	4	4	1
	E	C_4	C_4^2	σ	σ'	E	C_4	C_4^2	σ	σ	σ'	E	C_4^2	σ	σ'	E
	0	$0\theta\Omega$	0Ω	0Ω	$0\theta_\perp$	τ	τ	τ	$\tau_\parallel$	$\tau_\perp$	τ	θ	θ	θ	$\theta_\parallel\Omega$	Ω
Γ_1	1	1	1	1	1	1	1	1	1	1	1	1	1	1	1	1
Γ_2	1	1	1	-1	-1	1	1	1	-1	-1	-1	1	1	-1	-1	1
Γ_3	1	-1	1	1	-1	1	-1	1	1	1	-1	1	1	1	-1	1
Γ_4	1	-1	1	-1	1	1	-1	1	-1	-1	1	1	1	-1	1	1
Γ_5	2	0	-2	0	0	2	0	-2	0	0	0	2	-2	0	0	2
M_1	1	1	1	1	1	-1	-1	-1	-1	-1	-1	1	1	1	1	1
M_2	1	1	1	-1	-1	-1	-1	-1	1	1	1	1	1	-1	-1	1
M_3	1	-1	1	1	-1	-1	1	-1	-1	-1	1	1	1	1	-1	1
M_4	1	-1	1	-1	1	-1	1	-1	1	1	-1	1	1	-1	1	1
M_5	2	0	-2	0	0	-2	0	2	0	0	0	2	-2	0	0	2
X_1	2	0	2	2	0	0	0	0	0	0	0	-2	-2	-2	0	2
X_2	2	0	2	-2	0	0	0	0	0	0	0	-2	-2	2	0	2
X_3	2	0	-2	0	0	0	0	0	-2	2	0	-2	2	0	0	2
X_4	2	0	-2	0	0	0	0	0	2	-2	0	-2	2	0	0	2
Σ_1	4	0	0	0	2	0	0	0	0	0	0	0	0	0	-2	-4
Σ_2	4	0	0	0	-2	0	0	0	0	0	0	0	0	0	2	-4

(Table III)

Table IV. Class structure and group elements of the 128 element cluster-permutation group of the ordinary Hubbard model. The element P corresponds to the transposition of site-1 and site-5. The notation is identical to that of Table III.

class	group elements			size of class
1	$\{E\,\vert 0\}$			1
2	$\{C_4\vert 0,\theta,\Omega\}$			8
3	$\{C_4^2\vert 0,\Omega\}$			2
4	$\{\sigma\vert 0,\Omega\}$			4
5	$\{\sigma'\vert 0,\theta_\perp\}$			4
6	$\{E\,\vert\tau\}$,	$\{\sigma\vert\tau_\perp\}$		8
7	$\{C_4\vert\tau\}$,	$\{\sigma'\vert\tau\}$		16
8	$\{C_4^2\vert\tau\}$,	$\{\sigma\vert\tau_\parallel\}$		8
9	$\{E\,\vert\theta\}$,	$\{C_4^2\vert\theta\}$		4
10	$\{\sigma\vert\theta\}$			4
11	$\{\sigma'\vert\theta_\parallel,\Omega\}$			4
12	$\{E\,\vert\Omega\}$			1
13	$P\{E\,\vert 0\}$,	$P\{C_4^2\vert\Omega\}$,	$P\{\sigma\vert\Omega\}$	4
14	$P\{C_4\vert 0\}$,	$P\{\sigma'\vert\theta_\parallel\}$		4
15	$P\{C_4^2\vert 0\}$,	$P\{\sigma\vert 0\}$,	$P\{E\,\vert\Omega\}$	4
16	$P\{\sigma'\vert 0,\Omega\}$,	$P\{C_4\vert\theta\}$		8
17	$P\{E\,\vert\tau\}$,	$P\{C_4^2\vert\tau\}$,	$P\{\sigma\vert\tau\}$	16
18	$P\{C_4\vert\tau\}$,	$P\{\sigma'\vert\tau\}$		16
19	$P\{E\,\vert\theta\}$,	$P\{C_4^2\vert\theta\}$,	$P\{\sigma\vert\theta\}$	8
20	$P\{C_4\vert\Omega\}$,	$P\{\sigma'\vert\theta_\perp\}$		4

Table V. Character table of the 128 element cluster-permutation group for the ordinary Hubbard model. The class structure and group elements are given in Table IV. The classes are labeled by their number to save space in the table below. The last column gives the compatibility relations with the irreducible representations of the real space group (Table III). The subscripts p, z, and n denote representations that have a positive character, zero character, or negative character, respectively, for the element $P\{E|0\}$. The symbol ϕ is used to denote representations that mix different wavevectors.

(Table V)

	1	8	2	4	4	8	16	8	4	4	4	1	4	4	4	8	16	16	8	4	
	c_1	c_2	c_3	c_4	c_5	c_6	c_7	c_8	c_9	c_{10}	c_{11}	c_{12}	c_{13}	c_{14}	c_{15}	c_{16}	c_{17}	c_{18}	c_{19}	c_{20}	
Γ_{1p}	1	1	1	1	1	1	1	1	1	1	1	1	1	1	1	1	1	1	1	1	Γ_1
Γ_{1n}	1	1	1	1	1	1	1	1	1	1	1	1	-1	-1	-1	-1	-1	-1	-1	-1	Γ_1
Γ_{3p}	1	-1	1	1	-1	1	-1	1	1	1	-1	1	1	-1	1	-1	1	-1	1	-1	Γ_3
Γ_{3n}	1	-1	1	1	-1	1	-1	1	1	1	-1	1	-1	1	-1	1	-1	1	-1	1	Γ_3
M_{1p}	1	1	1	1	1	-1	-1	-1	1	1	1	1	1	1	1	1	-1	-1	1	1	M_1
M_{1n}	1	1	1	1	1	-1	-1	-1	1	1	1	1	-1	-1	-1	-1	1	1	-1	-1	M_1
M_{3p}	1	-1	1	1	-1	-1	1	-1	1	1	-1	1	1	-1	1	-1	-1	1	1	-1	M_3
M_{3n}	1	-1	1	1	-1	-1	1	-1	1	1	-1	1	-1	1	-1	1	1	-1	-1	1	M_3
ϕ_1	2	2	2	-2	-2	0	0	0	2	-2	-2	2	0	0	0	0	0	0	0	0	$\Gamma_2 \oplus M_2$
ϕ_2	2	-2	2	-2	2	0	0	0	2	-2	2	2	0	0	0	0	0	0	0	0	$\Gamma_4 \oplus M_4$
X_{1p}	2	0	2	2	0	0	0	0	-2	-2	0	2	2	0	2	0	0	0	-2	0	X_1
X_{1n}	2	0	2	2	0	0	0	0	-2	-2	0	2	-2	0	-2	0	0	0	2	0	X_1
X_{2z}	2	0	2	-2	0	0	0	0	-2	2	0	2	0	2	0	-2	0	0	0	2	X_2
X_{2z}'	2	0	2	-2	0	0	0	0	-2	2	0	2	0	-2	0	2	0	0	0	-2	X_2
ϕ_3	4	0	-4	0	0	2	0	-2	0	0	0	4	0	0	0	0	0	0	0	0	$\Gamma_5 \oplus X_3$
ϕ_4	4	0	-4	0	0	-2	0	2	0	0	0	4	0	0	0	0	0	0	0	0	$M_5 \oplus X_4$
Σ_{1p}	4	0	0	0	2	0	0	0	0	0	-2	-4	2	-2	-2	0	0	0	0	2	Σ_1
Σ_{1n}	4	0	0	0	2	0	0	0	0	0	-2	-4	-2	2	2	0	0	0	0	-2	Σ_1
Σ_{2p}	4	0	0	0	-2	0	0	0	0	0	2	-4	2	2	-2	0	0	0	0	-2	Σ_2
Σ_{2n}	4	0	0	0	-2	0	0	0	0	0	2	-4	-2	-2	2	0	0	0	0	2	Σ_2

Table VI. Character table for the space group of the eight-site rectangular-lattice cluster (chiral Hubbard model). The notation for the space group operations is the same as in Table III.

	1	2	2	2	1
	E	C_2	E	C_2	E
	0	0Ω	τ	τ	Ω
Γ_1	1	1	1	1	1
Γ_2	1	-1	1	-1	1
X_1	1	1	-1	-1	1
X_2	1	-1	-1	1	1
Σ_1	2	0	0	0	-2

Table VII. Class structure and group elements of the 32 element gauge-space group of the chiral Hubbard model (for an even number of electrons). The gauge factors χ_i are recorded in (12). The group elements without any gauge factors form a subgroup corresponding to the space group of Table VI.

class	group elements	size of class
1	$\{E \mid 0\}$	1
2	$\{C_4^2 \mid 0, \Omega\}$	2
3	$\chi_1\{C_4 \mid 0, \Omega\}$, $\chi_2\{C_4 \mid \theta_3, \theta_7\}$	4
4	$\chi_1\{C_4^3 \mid 0, \Omega\}$, $\chi_2\{C_4^3 \mid \theta_3, \theta_7\}$	4
5	$\{E \mid \tau_2, \tau_6\}$, $\chi_3\{E \mid \tau_4, \tau_8\}$	4
6	$\{C_4^2 \mid \tau_2, \tau_6\}$, $\chi_3\{C_4^2 \mid \tau_4, \tau_8\}$	4
7	$\chi_2\{C_4 \mid \tau_2, \tau_6\}$, $\chi_1\{C_4 \mid \tau_4, \tau_8\}$	4
8	$\chi_2\{C_4^3 \mid \tau_2, \tau_6\}$, $\chi_1\{C_4^3 \mid \tau_4, \tau_8\}$	4
9	$\chi_3\{E \mid \theta_3, \theta_7\}$	2
10	$\chi_3\{C_4^2 \mid \theta_3, \theta_7\}$	2
11	$\{E \mid \Omega\}$	1

Table VIII. Character table of the 32 element gauge-space group for the even-electron-number sector of the chiral Hubbard model. The class structure and group elements are given in Table VII. The gauge factors have been suppressed to save space in the table below. The last column gives the compatibility relations with the irreducible representations of the real space group (Table VI).

	1	2	4	4	4	4	4	4	2	2	1	
	E	C_4^2	C_4	C_4^3	E	C_4^2	C_4	C_4^3	E	C_4^2	E	
	0	0Ω	$0\theta\Omega$	$0\theta\Omega$	τ	τ	τ	τ	θ	θ	Ω	
γ_1	1	1	1	1	1	1	1	1	1	1	1	Γ_1
γ_2	1	1	-1	-1	1	1	-1	-1	1	1	1	Γ_1
γ_3	1	-1	i	$-i$	1	-1	i	$-i$	1	-1	1	Γ_2
γ_4	1	-1	$-i$	i	1	-1	$-i$	i	1	-1	1	Γ_2
m_1	1	1	1	1	-1	-1	-1	-1	1	1	1	X_1
m_2	1	1	-1	-1	-1	-1	1	1	1	1	1	X_1
m_3	1	-1	i	$-i$	-1	1	$-i$	i	1	-1	1	X_2
m_4	1	-1	$-i$	i	-1	1	i	$-i$	1	-1	1	X_2
x_1	2	2	0	0	0	0	0	0	-2	-2	2	$\Gamma_1 \oplus X_1$
x_2	2	-2	0	0	0	0	0	0	-2	2	2	$\Gamma_2 \oplus X_2$
σ_1	4	0	0	0	0	0	0	0	0	0	-4	$\Sigma_1 \oplus \Sigma_1$

Table IX. Reduced Hamiltonian block sizes for the ordinary Hubbard model. The largest block size is ${}^3\Sigma_{1p}$ (78×78). The numbers highlighted in bold indicate blocks that are further reducible by a hidden parameter-independent symmetry.[44–46]

spin	Γ_{1p}	Γ_{1n}	Γ_{3p}	Γ_{3n}	M_{1p}	M_{1n}	M_{3p}	M_{3n}	ϕ_1	ϕ_2	X_{1p}	X_{1n}	X_{2z}	X_{2z}'	ϕ_3	ϕ_4	Σ_{1p}	Σ_{1n}	Σ_{2p}	Σ_{2n}
4	0	1	0	0	0	0	0	0	0	0	0	0	0	0	0	0	0	0	0	0
3	0	3	0	1	0	4	0	1	0	1	0	5	0	1	1	1	0	6	0	2
2	1	**14**	2	12	0	11	1	9	11	14	1	**20**	9	12	21	25	10	**32**	14	32
1	15	**18**	18	16	16	**21**	19	19	37	**34**	35	**40**	43	**32**	75	71	78	**72**	74	72
0	36	**16**	22	13	30	**10**	18	9	20	35	48	**19**	20	27	47	55	68	**46**	60	42

Table X. Reduced Hamiltonian block sizes for the chiral Hubbard model. Note that the complex representation pairs (γ_3, γ_4) and (m_3, m_4) have not been separated.[37] The largest block size is ${}^3\sigma_1$ (296 × 296).

spin	γ_1	γ_2	γ_3 and γ_4	m_1	m_2	m_3 and m_4	x_1	x_2	σ_1
4	1	0	0	0	0	0	0	0	0
3	3	2	2	4	2	2	6	2	8
2	26	28	42	22	24	50	42	46	88
1	70	68	150	74	72	142	150	146	296
0	72	70	94	60	62	110	114	102	216

Table XI. Class structure and group elements of the 64 element full gauge-space group of the chiral Hubbard model. The gauge factors χ_i are recorded in (A.1). The barred elements correspond to the unbarred elements multiplied by $\{\bar{E}|0\}$. Classes 5, 6, and 9 include both barred and unbarred elements.

class	group elements				size of class
1	$\{E\|0\}$				1
2	$\{C_4^2\|0,\Omega\}$				2
3	$\chi_1\{C_4\|0\}$,	$\chi_2\{C_4\|\theta_3\}$,	$\chi_5\{C_4\|\theta_7\}$,	$\chi_6\{C_4\|\Omega\}$	4
4	$\chi_1\{C_4^3\|0\}$,	$\chi_5\{C_4^3\|\theta_3\}$,	$\chi_2\{C_4^3\|\theta_7\}$,	$\chi_6\{C_4^3\|\Omega\}$	4
5	$\{E,\bar{E}\|\tau_2,\tau_6\}$,	$\chi_3\{E,\bar{E}\|\tau_4,\tau_8\}$			8
6	$\{C_4^2,\bar{C}_4^2\|\tau_2,\tau_6\}$,	$\chi_3\{C_4^2,\bar{C}_4^2\|\tau_4,\tau_8\}$			8
7	$\chi_2\{C_4\|\tau_2,\tau_6\}$,	$\chi_1\{C_4\|\tau_4,\tau_8\}$			4
8	$\chi_2\{C_4^3\|\tau_2,\tau_6\}$,	$\chi_1\{C_4^3\|\tau_4,\tau_8\}$			4
9	$\chi_3\{E,\bar{E}\|\theta_3,\theta_7\}$				4
10	$\chi_4\{C_4^2\|\theta_3\}$,	$\chi_3\{C_4^2\|\theta_7\}$			2
11	$\{E\|\Omega\}$				1
12	$\{\bar{E}\|0\}$				1
13	$\{\bar{C}_4^2\|0,\Omega\}$				2
14	$\chi_1\{\bar{C}_4\|0\}$,	$\chi_2\{\bar{C}_4\|\theta_3\}$,	$\chi_5\{\bar{C}_4\|\theta_7\}$,	$\chi_6\{\bar{C}_4\|\Omega\}$	4
15	$\chi_1\{\bar{C}_4^3\|0\}$,	$\chi_5\{\bar{C}_4^3\|\theta_3\}$,	$\chi_2\{\bar{C}_4^3\|\theta_7\}$,	$\chi_6\{\bar{C}_4^3\|\Omega\}$	4
16	$\chi_2\{\bar{C}_4\|\tau_2,\tau_6\}$,	$\chi_1\{\bar{C}_4\|\tau_4,\tau_8\}$			4
17	$\chi_2\{\bar{C}_4^3\|\tau_2,\tau_6\}$,	$\chi_1\{\bar{C}_4^3\|\tau_4,\tau_8\}$			4
18	$\chi_4\{\bar{C}_4^2\|\theta_3\}$,	$\chi_3\{\bar{C}_4^2\|\theta_7\}$			2
19	$\{\bar{E}\|\Omega\}$				1

Table XII. Character table of the 64 element full gauge-space group for the chiral Hubbard model. The class structure and group elements are given in Table XI. The eleven "single-valued" representations are recorded in Table VIII. Only the eight "double-valued" representations are recorded here. The gauge factors have been suppressed to save space in the table below. The last column gives the compatibility relations with the irreducible representations of the real space group (Table VI). The symbol $\alpha = (1+i)/\sqrt{2}$ is used to denote the square root of i.

	1	2	4	4	8	8	4	4	4	2	1	1	2	4	4	4	4	2	1	
	E	C_4^2	C_4	C_4^3	$E\bar{E}$	$C_4^2\bar{C}_4^2$	C_4	C_4^3	$E\bar{E}$	C_4^2	E	$\bar{E}$	$\bar{C}_4^2$	$\bar{C}_4$	$\bar{C}_4^3$	$\bar{C}_4$	$\bar{C}_4^3$	$\bar{C}_4^2$	$\bar{E}$	
	0	0Ω	$0\theta\Omega$	$0\theta\Omega$	τ	τ	τ	τ	θ	θ	Ω	0	0Ω	$0\theta\Omega$	$0\theta\Omega$	τ	τ	θ	Ω	
ω_1	2	2	0	0	0	0	$\sqrt{2}$	$\sqrt{2}$	0	0	2	-2	-2	0	0	$-\sqrt{2}$	$-\sqrt{2}$	0	-2	$\Gamma_1 \oplus X_1$
ω_2	2	2	0	0	0	0	$-\sqrt{2}$	$-\sqrt{2}$	0	0	2	-2	-2	0	0	$\sqrt{2}$	$\sqrt{2}$	0	-2	$\Gamma_1 \oplus X_1$
ω_3	2	-2	0	0	0	0	$\sqrt{2}i$	$-\sqrt{2}i$	0	0	2	-2	2	0	0	$-\sqrt{2}i$	$\sqrt{2}i$	0	-2	$\Gamma_2 \oplus X_2$
ω_4	2	-2	0	0	0	0	$-\sqrt{2}i$	$\sqrt{2}i$	0	0	2	-2	2	0	0	$\sqrt{2}i$	$-\sqrt{2}i$	0	-2	$\Gamma_2 \oplus X_2$
ω_5	2	0	$\sqrt{2}\alpha$	$-\sqrt{2}\alpha^3$	0	0	0	0	0	$2i$	-2	-2	0	$-\sqrt{2}\alpha$	$\sqrt{2}\alpha^3$	0	0	$-2i$	2	Σ_1
ω_6	2	0	$-\sqrt{2}\alpha^3$	$\sqrt{2}\alpha$	0	0	0	0	0	$-2i$	-2	-2	0	$\sqrt{2}\alpha^3$	$-\sqrt{2}\alpha$	0	0	$2i$	2	Σ_1
ω_7	2	0	$-\sqrt{2}\alpha$	$\sqrt{2}\alpha^3$	0	0	0	0	0	$2i$	-2	-2	0	$\sqrt{2}\alpha$	$-\sqrt{2}\alpha^3$	0	0	$-2i$	2	Σ_1
ω_8	2	0	$\sqrt{2}\alpha^3$	$-\sqrt{2}\alpha$	0	0	0	0	0	$-2i$	-2	-2	0	$-\sqrt{2}\alpha^3$	$\sqrt{2}\alpha$	0	0	$2i$	2	Σ_1

Figure Captions

Figure 1. Eight-site square-lattice cluster with periodic boundary conditions for the ordinary Hubbard model in (a) real and (b) reciprocal space. The nearest-neighbor hopping is indicated in (a) by thick solid lines, the next-nearest-neighbor hopping by thin dashed lines (see Table I), and the primitive unit cell is highlighted in gray. Note that the four next-nearest neighbors of site 1 are *two* each of the sites 3 and 7. The four symmetry stars in (b) are $\Gamma = (0,0)$; $M = (1,1)\,\pi/a$; $X = (1,0)\,\pi/a$; and $\Sigma = (1,1)\,\pi/2a$.

Figure 2. Eight-site cluster with periodic boundary conditions for the chiral Hubbard model in (a) real and (b) reciprocal space. The nearest-neighbor hopping is indicated in (a) by thick solid lines ($-t$) and thick dotted lines ($+t$), and the next-nearest-neighbor hopping by thin dashed lines in the direction of the arrow ($+it$) and in the opposite direction of the arrow ($-it$) [see Table II]. The gauge is chosen so that each elementary triangle contains a flux of $\pi/2$, the nearest-neighbor hopping elements are real, and the next-nearest-neighbor hopping elements are imaginary. The rectangular primitive unit cell is highlighted in gray. The four wavevectors of the real space group are indicated by white dots in (b) and correspond to $\Gamma = (0,0)$; $X = (1,0)\,\pi/a$; and $\Sigma = (1,1)\,\pi/2a$, $(-1,1)\,\pi/2a$. The Brillouin zone for the chiral Hubbard model in the chosen gauge is highlighted in gray. The black dots in (b) correspond to the four additional gauge-wavevectors of the enlarged gauge-Brillouin zone for the gauge-space group of the chiral Hubbard model [see the description in (vii) of Section II].

Figure 3. Ground-state phase diagram for the ordinary Hubbard model at half filling ($N = M = 8$). The vertical axis records the relative hopping [Eq. (19)] and the horizontal axis records the interaction strength [Eq. (20)]. The labels denote the ground-state symmetry for each corresponding phase as given in Table V. The ground state is degenerate at $t' = t/2$: the dashed line (at small U)

corresponds to the ground state ${}^1\phi_2 \oplus {}^1\phi_4$ and the solid line (at large U) corresponds to the ground state ${}^1\Gamma_{1n} \oplus {}^1\Gamma_{1n} \oplus {}^1\Gamma_{3n}$. Note that the phase ${}^5\Sigma_{2n}$ is a *ferrimagnetic* ground state and the regions where adiabatic continuation is possible are $t' = 0$ and $t' > t$.

Figure 4. Spin-spin correlation functions L_i [Eq. (16a)] for three different values of t'/t in the ordinary Hubbard model. The value of the correlation function lies on the vertical axis and the interaction strength [Eq. (20)] lies on the horizontal axis. The labels 0 (on-site), 1 (nearest neighbor), 2 (next-nearest neighbor), and 3 (third-nearest neighbor) denote the subscript i. Discontinuities in the spin-spin correlation functions occur only at the level crossings (see Fig. 3). At large U the ground state is ordered as a two-sublattice Néel antiferromagnet ($t < t/2$) or a four-sublattice Néel antiferromagnet ($t' > t/2$). Note that the case with $t' = 0.95\,t$ includes the correlation functions for the magnetic phase at moderate values of U.

Figure 5. Number-number correlation functions N_i [Eq. (16c)] for three different values of t'/t in the ordinary Hubbard model. The vertical axis is the interaction strength [Eq. (20)] and the labels denote the subscript i. Note that $N_i \rightarrow 1$ when $U \rightarrow \infty$, as expected.

Figure 6. Ground-state phase diagram for the chiral Hubbard model at half-filling ($N = M = 8$). The vertical axis records the relative hopping [Eq. (19)] and the horizontal axis records the interaction strength [Eq. (20)]. The labels denote the ground-state symmetry for each corresponding phase as given in Table VIII. All ground states are spin singlets ($S = 0$), pseudospin singlets ($J = 0$), and have even particle-hole parity ($R = 1$). Adiabatic continuation is possible at three points: $t' = 0$; $t' = t/2$; and $t = 0$.

Figure 7. Spin-spin correlation functions L_i [Eq. (16a)] for three different values of t'/t in the chiral Hubbard model. The point $t' = 0.3\,t$ is representative of the

case $t' < t/2$ and the point $t' = 0.8t$ is representative of the case $t' > t/2$. The vertical axis plots the interaction strength [Eq. (20)] and the labels in the figures denote the subscript i. At large U the ground state is ordered as a two-sublattice Néel antiferromagnet ($t < t/2$) or a four-sublattice Néel antiferromagnet ($t' > t/2$). The point $t' = t/2$ is special and has intermediate-range antiferromagnetic order as $U \rightarrow \infty$. This may be a representative of a spin-liquid state for a finite system.

Figure 8. Number-number correlation functions N_i [Eq. (16c)] for $t' = 0.3t$ in the chiral Hubbard model. The other cases all have similar number-number correlation functions.

Figure 9. Spin-triple-product correlation function O_{124} [Eq. (16d)] for two values of t'/t in the chiral Hubbard model. The point $t' = 0.3t$ is representative of the general case where the sign of O_{124} changes and the magnitude decreases by a factor of ten at the level crossing between the ${}^1\gamma_2$ (small U) and the ${}^1\gamma_1$ (large U) ground state. Note that at the special point $t' = t/2$ (where there is no level crossing) O_{124} approaches zero with a finite slope as $U \rightarrow \infty$.

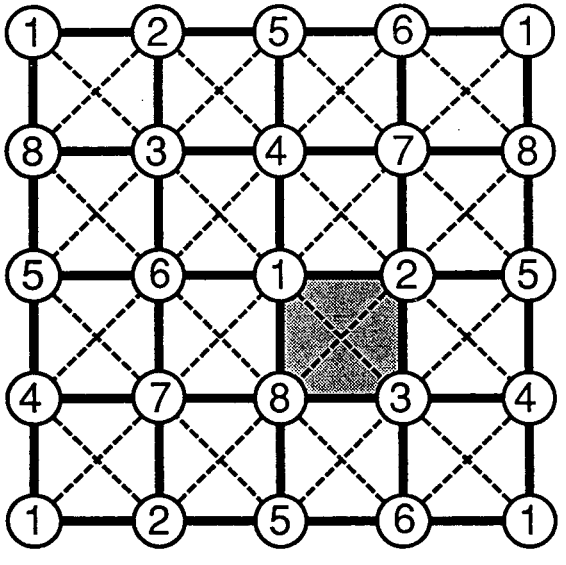

(a)

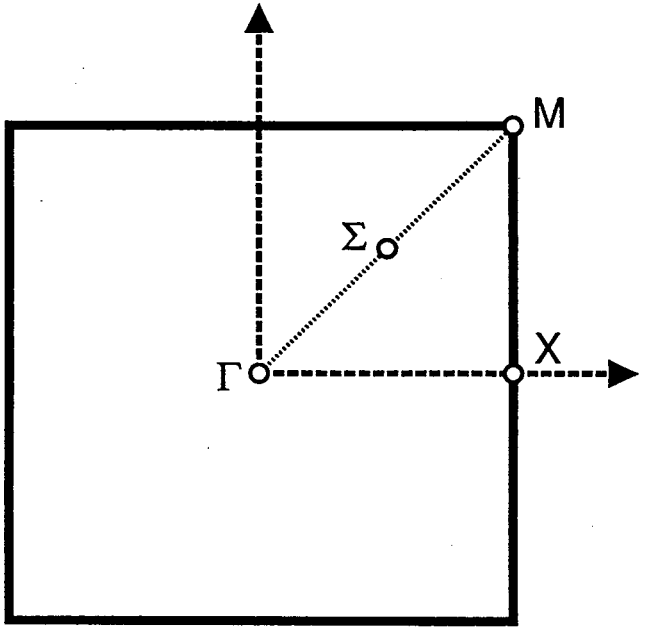

(b)

Figure 1

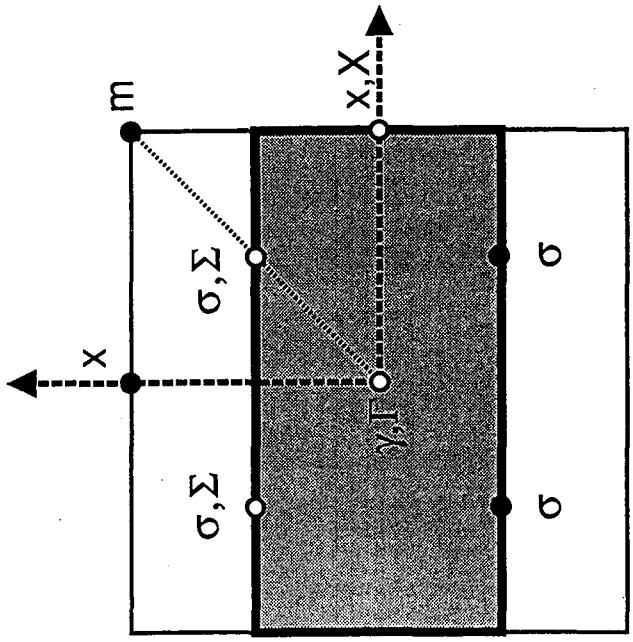

(b)

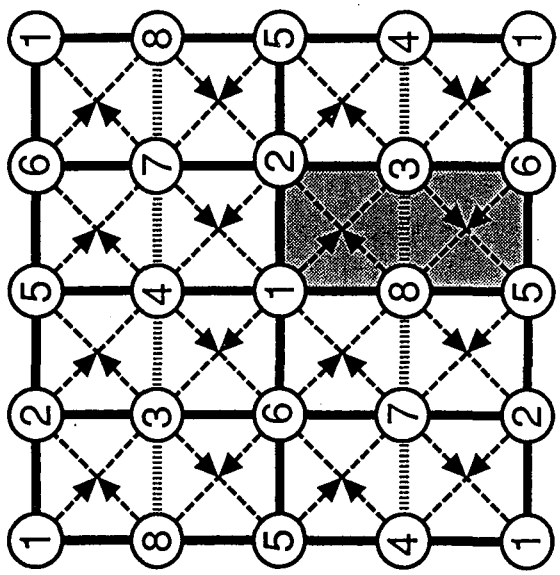

(a)

Figure 2

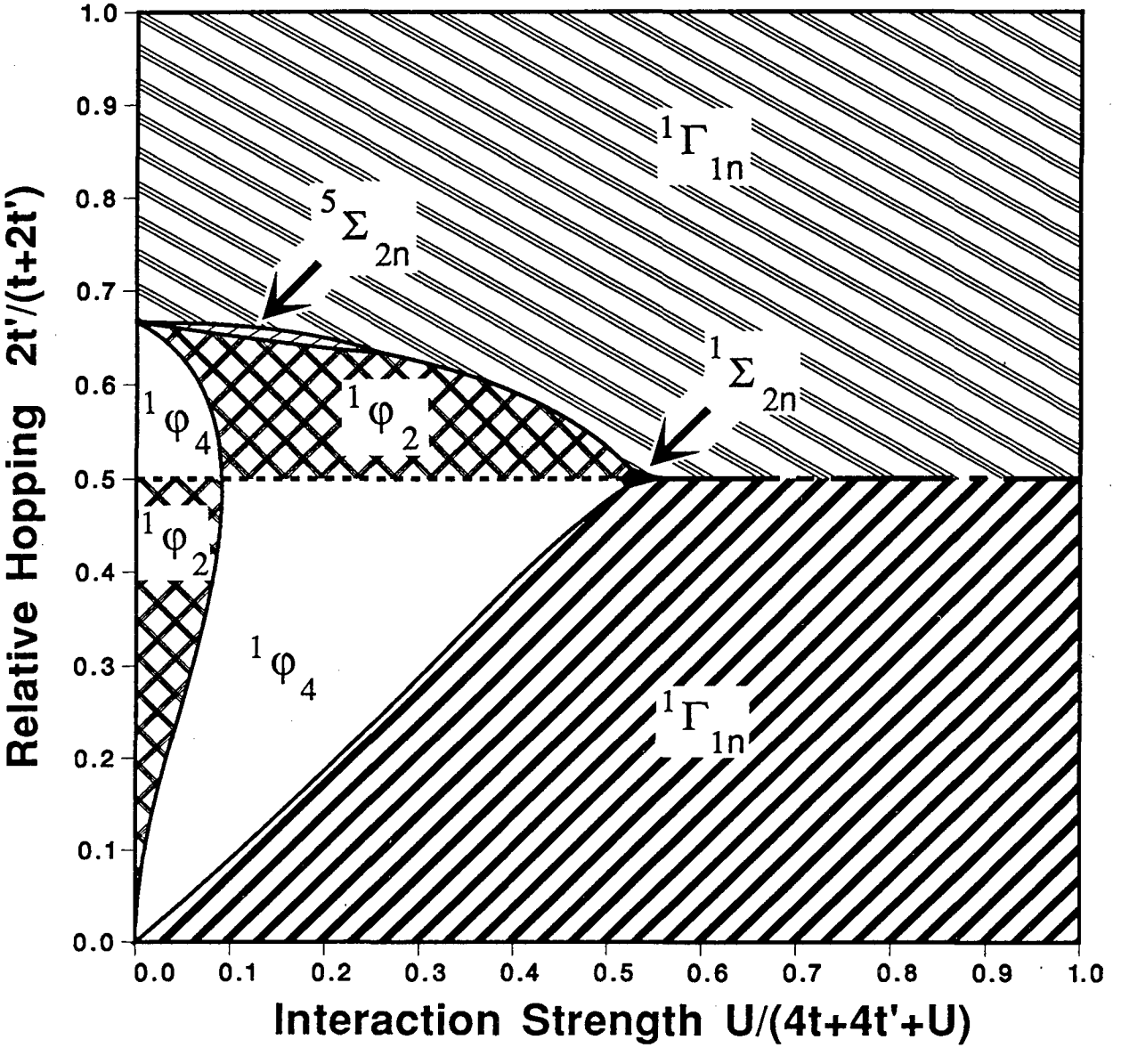
Relative Hopping 2t'/(t+2t')
Interaction Strength U/(4t+4t'+U)
1.0
0.9
0.8
0.7
0.6
0.5
0.4
0.3
0.2
0.1
0.0
0.0
0.1
0.2
0.3
0.4
0.5
0.6
0.7
0.8
0.9
1.0
$^1\Gamma_{1n}$
$^5\Sigma_{2n}$
$^1\Sigma_{2n}$
$^1\varphi_4$
$^1\varphi_2$
$^1\varphi_{2'}$
$^1\varphi_4$
$^1\Gamma_{1n}$

Figure 3

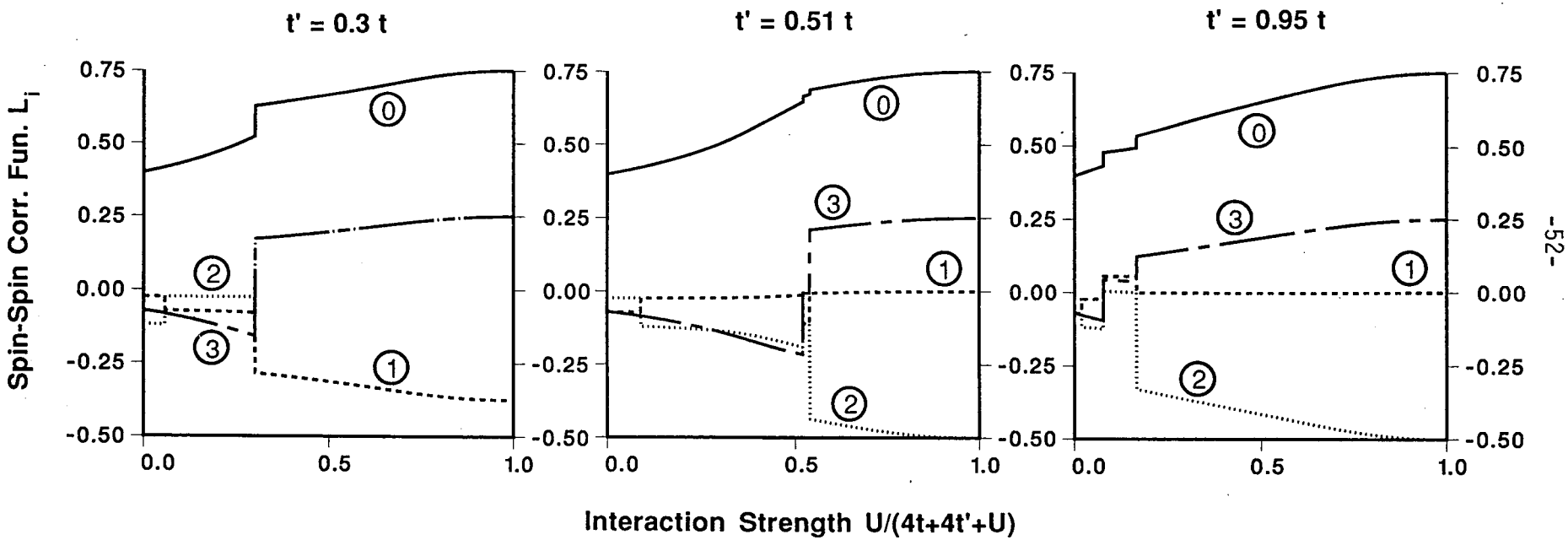
t' = 0.3 t
t' = 0.51 t
t' = 0.95 t
Spin-Spin Corr. Fun. L_i
0.75
0.50
0.25
0.00
-0.25
-0.50
0.0
0.5
1.0
0
1
2
3
Interaction Strength U/(4t+4t'+U)

Figure 4

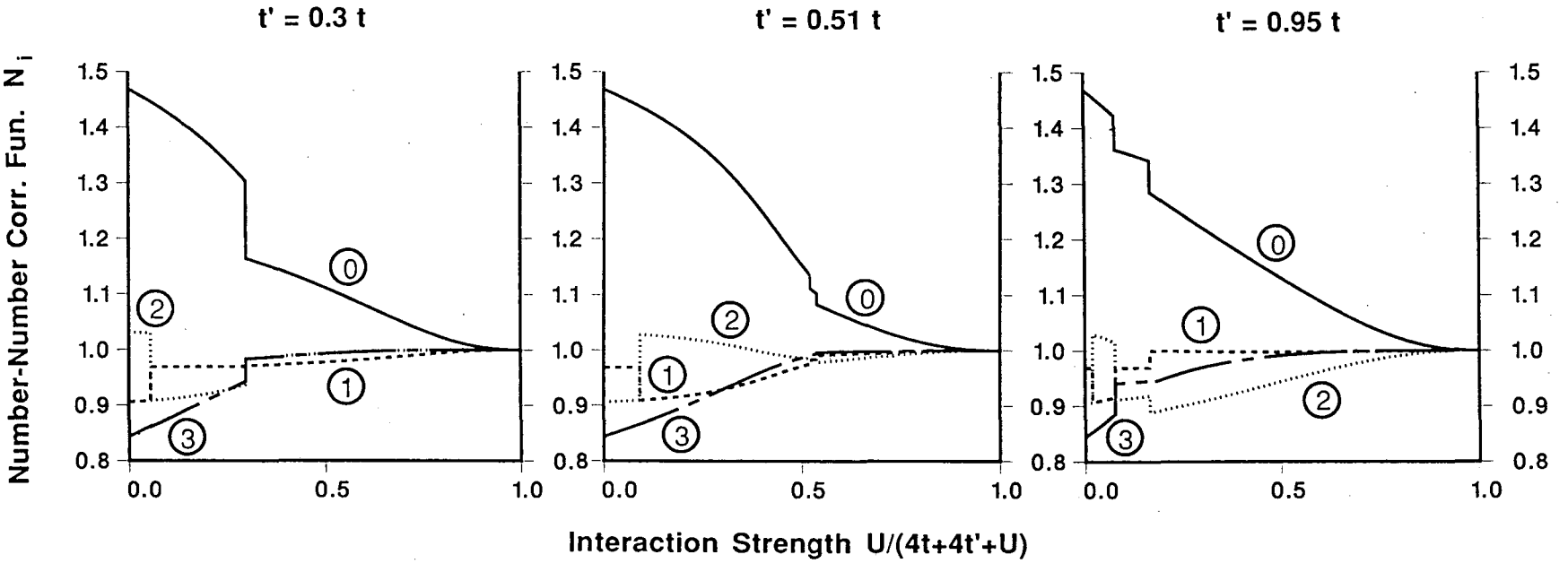
t' = 0.3 t
t' = 0.51 t
t' = 0.95 t
Number-Number Corr. Fun. N_i
1.5
1.4
1.3
1.2
1.1
1.0
0.9
0.8
0.0
0.5
1.0
0
1
2
3
Interaction Strength U/(4t+4t'+U)

Figure 5

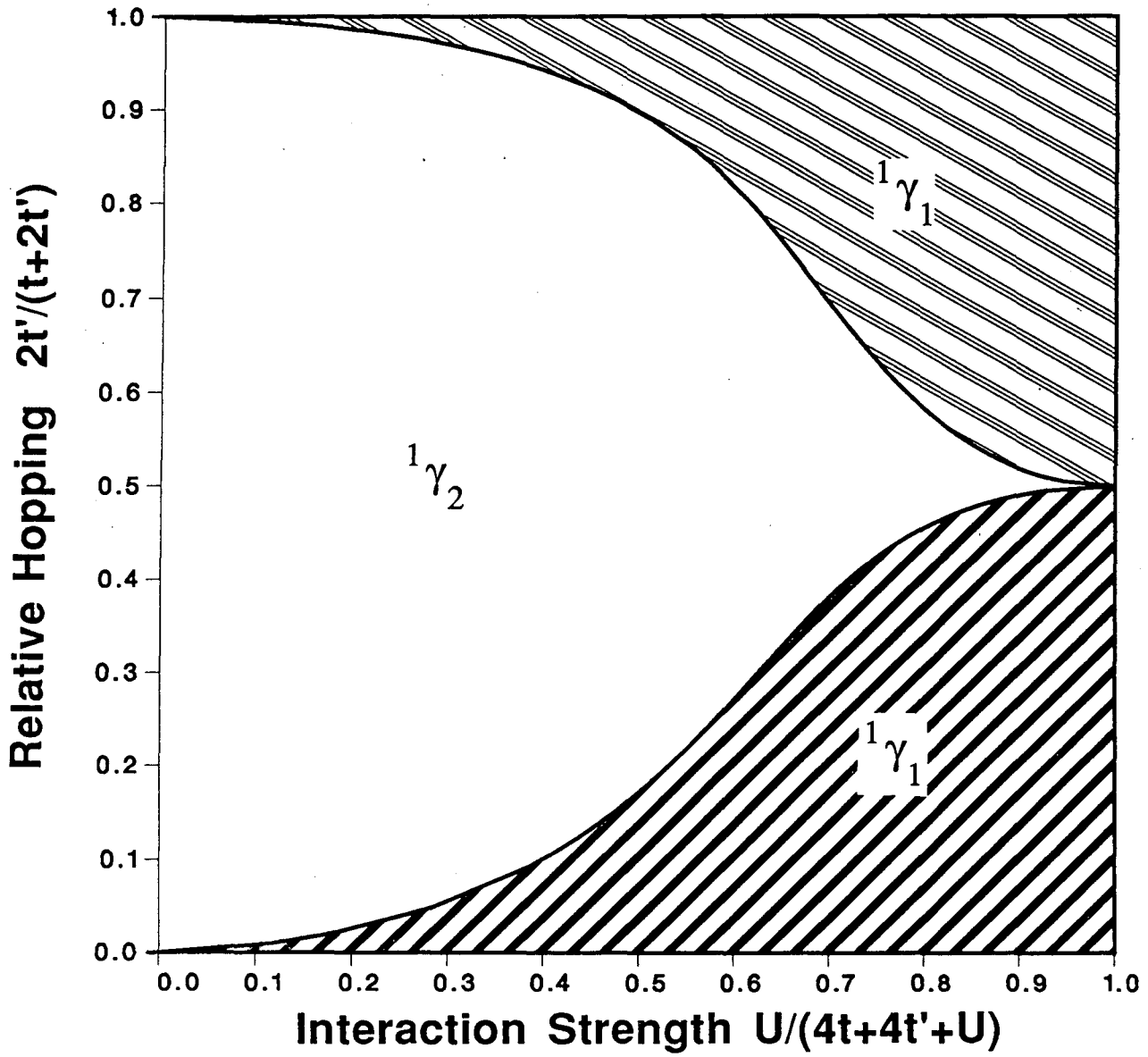
Relative Hopping 2t'/(t+2t')
Interaction Strength U/(4t+4t'+U)
1.0
0.9
0.8
0.7
0.6
0.5
0.4
0.3
0.2
0.1
0.0
0.0
0.1
0.2
0.3
0.4
0.5
0.6
0.7
0.8
0.9
1.0
$^1\gamma_1$
$^1\gamma_2$
$^1\gamma_1$

Figure 6

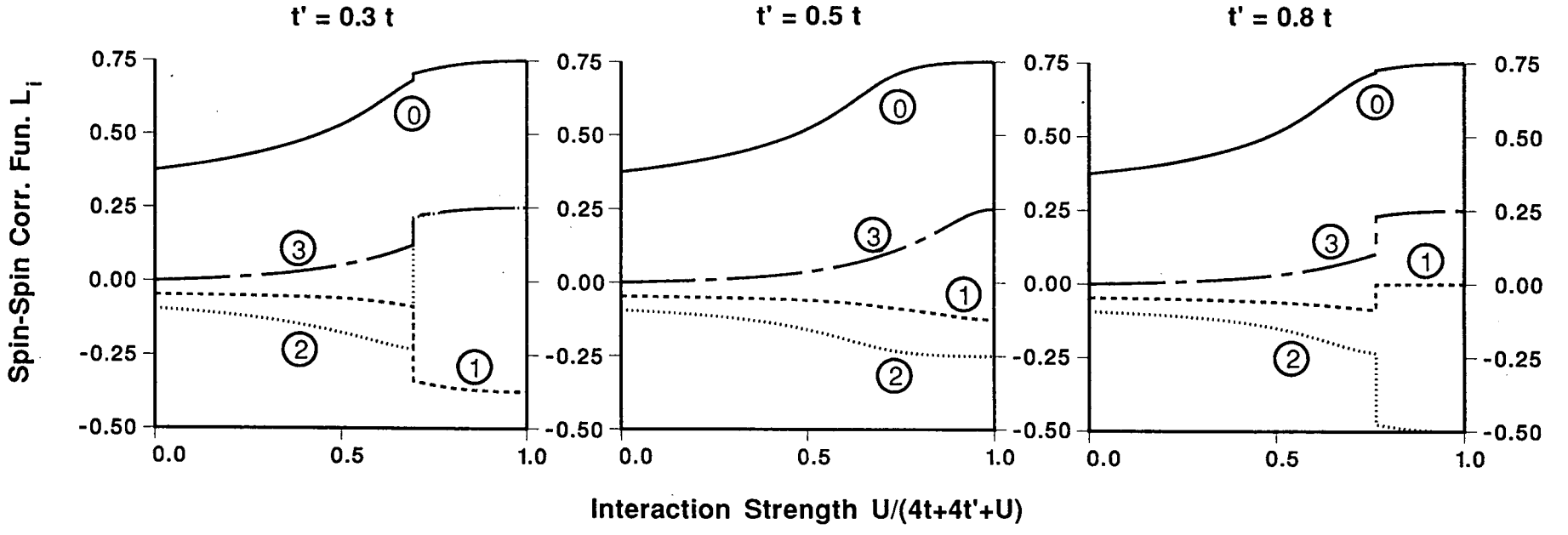
t' = 0.3 t
t' = 0.5 t
t' = 0.8 t
Spin-Spin Corr. Fun. L_i
0.75
0.50
0.25
0.00
-0.25
-0.50
0.0
0.5
1.0
0
1
2
3
Interaction Strength U/(4t+4t'+U)

Figure 7

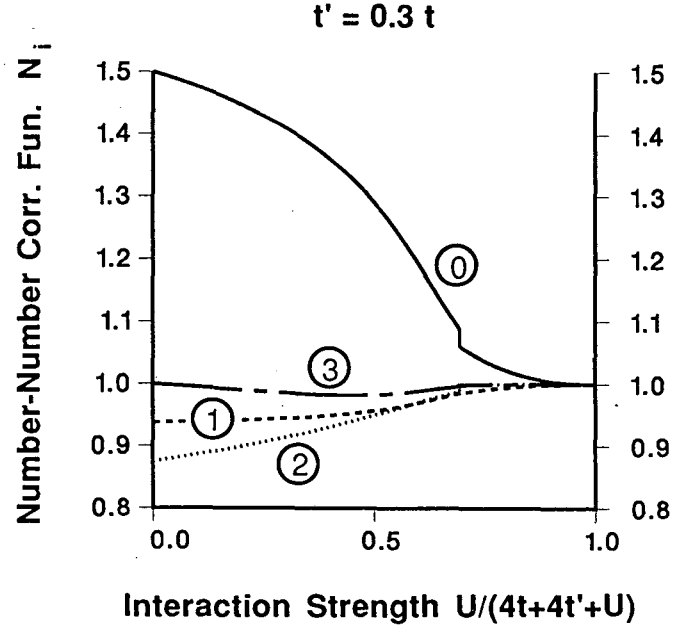
t' = 0.3 t
Number-Number Corr. Fun. N_i
1.5
1.4
1.3
1.2
1.1
1.0
0.9
0.8
0.0
0.5
1.0
0
1
2
3
Interaction Strength U/(4t+4t'+U)

Figure 8

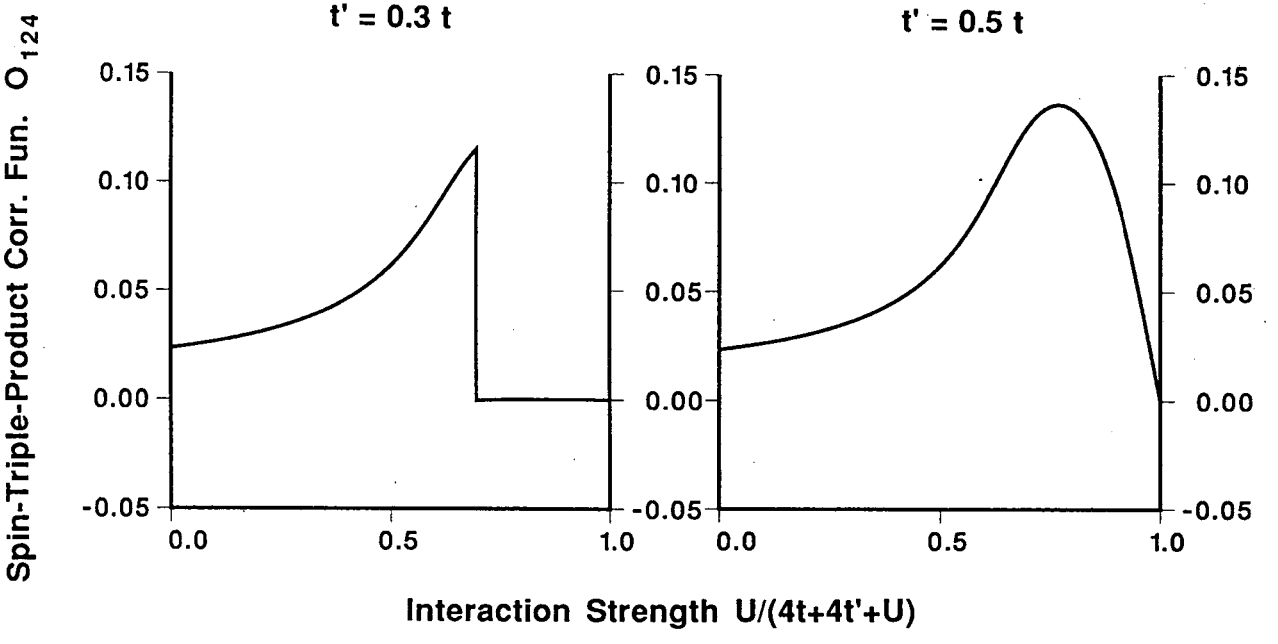
t' = 0.3 t
t' = 0.5 t
Spin-Triple-Product Corr. Fun. O_{124}
0.15
0.10
0.05
0.00
-0.05
0.0
0.5
1.0
Interaction Strength U/(4t+4t'+U)

Figure 9

LAWRENCE BERKELEY LABORATORY
UNIVERSITY OF CALIFORNIA
INFORMATION RESOURCES DEPARTMENT
BERKELEY, CALIFORNIA 94720